UAS-Based Archaeological Remote Sensing: Review, Meta-Analysis and State-of-the-Art

drones

MDPI

Review

UAS-Based Archaeological Remote Sensing: Review, Meta-Analysis and State-of-the-Art

Efstathios Adamopoulos [1,*] and Fulvio Rinaudo [2]

[1] Dipartimento di Informatica, Università degli Studi di Torino, Corso Svizzera 185, 10149 Torino, Italy
[2] Politecnico di Torino—DAD, Viale P.A. Mattioli, 39, 10125 Torino, Italy; fulvio.rinaudo@polito.it
* Correspondence: efstathios.adamopoulos@unito.it

Received: 6 August 2020; Accepted: 17 August 2020; Published: 19 August 2020

Abstract: Over the last decade, we have witnessed momentous technological developments in unmanned aircraft systems (UAS) and in lightweight sensors operating at various wavelengths, at and beyond the visible spectrum, which can be integrated with unmanned aerial platforms. These innovations have made feasible close-range and high-resolution remote sensing for numerous archaeological applications, including documentation, prospection, and monitoring bridging the gap between satellite, high-altitude airborne, and terrestrial sensing of historical sites and landscapes. In this article, we track the progress made so far, by systematically reviewing the literature relevant to the combined use of UAS platforms with visible, infrared, multi-spectral, hyper-spectral, laser, and radar sensors to reveal archaeological features otherwise invisible to archaeologists with applied non-destructive techniques. We review, specific applications and their global distribution, as well as commonly used platforms, sensors, and data-processing workflows. Furthermore, we identify the contemporary state-of-the-art and discuss the challenges that have already been overcome, and those that have not, to propose suggestions for future research.

Keywords: UAS; lightweight sensors; near-infrared sensors; thermal sensors; multi-spectral sensors; hyperspectral sensors; LiDAR; remote sensing; archaeology; prospection

1. Introduction

In the past decade, substantial technological progress has been recorded in the manufacturing of unmanned aerial platforms and affordable lightweight active and passive sensing devices, and the integration of microelectronics. Benefiting from the above, remotely controlled integrated sensing systems, which do not require an on-board crew, are being continuously miniaturized and have become widely accessible for commercial use. The development of integrated unmanned aircraft system (UAS)-based solutions is increasingly providing researchers with means to capture remote sensing data for archaeological applications, at spectral, spatial, and temporal resolutions not achievable with satellite or manned systems. UAS-based data collection is consistently becoming cost-effective given the unprecedented increase of precision and accuracy, and the ever-present capacity to cover vast, often inaccessible historical sites, of varying topographical characteristics with shorter flights and with less time-consuming acquisition planning. Thus, implementations of UAS for archaeology aim to fill in the existing gap between satellite/airborne sensing and terrestrial archaeological investigations.

The scope and spatiotemporal characteristics of an archaeological application are determinant for the optimal combination of platforms, sensing payloads, and processing techniques. This paper aims to present a comprehensive survey of the archaeological UAS-based remote sensing approaches reported in recent literature and gives a detailed account of the current state-of-the-art on relevant sensors, integrated payloads, and aerial platforms. The conducted research tracks the integration of technological advancements made during the last decade—on uncrewed platforms, lightweight

sensors, and post-processing techniques—in UAS-based remote-sensing archaeological activities, in order to identify occurred opportunities and challenges and to express future perspectives.

Organization of the Article

This paper provides a systematic review and meta-analysis of UAS-based hardware, software, and data analysis scenarios relevant to archaeological applications of remote sensing. Section 2 provides a brief overview of the development of archaeological remote sensing and identifies the problems for which UAS-based data collection is called to provide solutions. Section 3 addresses the methodology of the presented survey. Section 4 describes and analyzes the results of the systematic review. Specifically, Section 4.1 reports on utilized platforms, Section 4.2 on navigation parameters, Section 4.3 on sensors, and Section 4.4 on the reported cases of the applied archaeological remote sensing, and the relevant data products. Section 5 discusses the current state-of-the-art regarding UAS-based remote sensing. Finally, Section 6 presents some concluding remarks and perspectives.

2. Background

Traditional aerial imagery—produced with optical sensors—has proven to be beneficial to many archaeological applications. For more than eight decades, it has systematically provided an effective solution for settlement and landscape archaeology [1–3], which has recently been combined with other non-destructive archaeological methods [4–7]. Aerial RGB imaging has been implemented in different scenarios to identify earthworks and remains that are still just observable above the ground level: by exploiting the differential shadow and highlight effects when the sun is low in the sky, the effects of melting snow and widespread flooding, as well as the existence of positive/negative cropmarks and soilmarks through identifying color differentiation from the surroundings [8,9].

Archaeological remote- (and close-range) sensing activities, especially concerning fully buried historical remains, depend considerably on the quantization of the contrast within their immediate context, which is often not found at the visible (VIS) spectrum. Since archaeological remains do not present spectral signatures useful for generic detection applications, it is hypothesized that they exhibit localized contrasts in the landscape matrix, detectable using suitable sensors under appropriate environmental conditions. The measurement of the desired contrast can be realized directly, when there are detectable topographic effects, or indirectly, when variations of vegetation, magnetic fields, electrical properties, thermal behavior, or spectral reflectance exist [10–13].

Airborne light detection and ranging (LiDAR) has emerged as a prevalent active remote sensing technique for the direct measurement of the effects that close-to-surface buried archaeological remains have on the topography of a landscape. Laser-based sensors are capable of providing the needed primary data for detailed digital terrain and surface models (DTM, DSM) over vast landscapes, which, if subjected to appropriate artificial hill-shading, can assist the interpretation of significantly more features than with original aerial surveys [14,15]. Furthermore, LiDAR has the ability to penetrate foliage, making it particularly useful for vegetated landscapes, such as tropical regions where rapid vegetative growth can obscure the microtopography of archaeologically rich terrain [16,17]. The artificially shaded visualization of LiDAR-produced DTMs or (the unfiltered from canopy) DSMs, which has been explored according to slope, aspect, principal component analysis (PCA), local relief modeling (LRM), sky-view factor (SVF), and trend removal [18,19] can further increase the visibility of archaeological features.

The detection of the landscape matrix contrast that can indirectly provide interpretations of archaeological significance, requires data from various small components of the electromagnetic spectrum, making multi-spectral and hyperspectral-sensor approaches particularly pertinent for comprehensive surveys. Towards this end, satellite imaging has contributed significantly to archaeological research since high-resolution satellite datasets became available for commercial use [20–22]. The level of difference between the electromagnetic energy reflected and/or emitted from a feature and the background energy—as registered by the multi-spectral or hyperspectral

sensor—determines the successful location and analysis of the feature [23]. The main techniques used in archaeology for the analysis of multi-spectral imagery are visual interpretation, false color composite visualizations, vegetation and soil indices, thresholding, classification, PCA, filtering, and Geographic Information Systems (GIS) [20,23,24]. Occasionally, airborne multisensory apparatuses have been involved for archaeological surveys to simulate multiwavelength imagery acquired from satellite-based sensors [25–27]. Aerial thermography, to an extent, has also been employed for archaeological remote sensing [28,29] for the detection of measurably distinct variations between the features and the soil matrix in which they are embedded. Furthermore, case studies of archaeological aerial thermography with higher spatial and spectral resolution sensors have been recently reported [30,31].

Satellite and manned aircraft system-based remote sensing includes expensive platforms, which are significantly restrictive due to availability limitations and/or complex logistics. Moreover, satellite, and airborne imaging and LiDAR, come with noteworthy drawbacks concerning spatial and temporal resolution, and the flexibility of data acquisition [32,33]. Low-altitude nadiral photography, as an alternative to satellite and airborne-sensing approaches, has a long tradition of implementation for archaeological applications employing unmanned aerial platforms [34–36], with notably varying capabilities, maximum payloads, working heights, optimal operation conditions and flexibility.

The recent technological developments in UAS-borne integrated multi-sensor systems have provided us with powerful solutions for archaeological sensing, with enhanced maneuverability, spectral range, data precision, and navigational accuracy [37–39]. Compared to manned aerial platforms, unmanned aircraft can generally be operated with higher consistency and stability, under varying conditions and over a plethora of topographies [40–43]. Therefore, they are called to bridge the gap between satellite, airborne and terrestrial techniques in terms of spatial and temporal resolution, and to provide easy-to-use solutions for a variety of heritage specialists [44–46]. After almost a decade of UAS-based archaeological remote sensing, it is an opportune time to review the platforms, the payloads, and the processing techniques involved so far over various applications, and to record the current state-of-the-art at the turn of the new decade.

3. Methodology

3.1. Article Selection Method

To complete the presented review and meta-analysis a thorough literature search was undertaken on UAS-based applications for archaeological remote sensing up to 18th June 2020, in line with related studies [47,48]. The search was done using the Google Scholar platform, and produced 272 results. Keywords for the search included drones in their various meanings and acronyms: “unmanned aircraft system”, “unmanned aerial system”, “UAS”, “unmanned aerial vehicle” [UAV], “uncrewed aerial vehicle”, “UAV”, “remotely piloted aerial system”, “RPAS”, “drone”. These were combined with terms referring to sensing, sensors, and typical archaeological applications: “remote sensing”, “low-altitude sensing”, “near-infrared”, “thermal”, “multi-spectral”, “hyperspectral”, “laser scanner”, “LiDAR”, “GPR” [ground-penetrating radar], “photogrammetry”, “heritage”, “archaeology”, “archaeological site”, “archaeological landscape”, “archaeological remains”, “buried remains”, “historical landscape”, “archaeological prospection”, and “heritage diagnostics”. In total, 65 combinations were applied using logical disjunctions. This was further complemented through reference harvesting, citation tracking, choosing abstracts from relevant conference programs, and author search using Scopus and ResearchGate, which produced an additional 30 records.

Duplicate results and results that were insufficiently relevant to archaeological research were removed, which reduced the number of results to 231. The publications were collated and revised accordingly, after full-manuscript reading (see PRISMA flowchart in Supplementary Figure S1 checklist). The initial results were filtered according to document type. Peer-reviewed publications not reporting the use of UAS platforms or reporting the use of UAS-based imaging only as a complementary documentation means for satellite/airborne sensing were not considered. It should be highlighted

that the current study also did not consider applications of metric or non-metric documentation surveys that were purposed for merely creating three-dimensional (3D) photorealistic records of archaeological remains. Therefore, articles reporting this typology of studies were discarded. Furthermore, peer-reviewed publications that solely reported the use of images as-shot with no post-processing taking place were also discarded. The final list of selected publications consisted of 68 records related to UAS-based archaeological remote-sensing applications, reporting 78 distinct studies (meaning morphologically vastly different sites or the implementation of different survey workflows). The final list included 45 journal articles, 12 conference proceedings papers, and one book chapter (see Supplementary File S2).

3.2. Content Meta-Analysis

The studies were classified into four categories that correspond to representative archaeological remote-sensing fields. The categories are: "archaeological prospection" for studies aimed at the detection of buried archaeological remains either by direct sensing of their properties, or by measuring the contrast within their immediate landscape matrix (number = 60); "historical terrain visualization" for applications related to digitally enhancing the visibility of observable above ground archaeological features such as previously unburied remains, earthworks or geoglyphs, and of their immediate surroundings (number = 18); "archaeogeography" for studies directed towards analyzing the detected archaeological features—beyond plain visualization—by defining their geospatial relations (number = 7); "site monitoring" for those investigations aimed at monitoring historical landscapes and uncovering their natural or human-induced historical transformations through time (number = 4). For a few cases, an overlap was observed (number = 15), meaning simultaneous use of the same UAS-based equipment for more than one archaeological purpose, with different platform configurations, or by exploiting multiple data-processing scenarios.

For the meta-analysis, various parameters were catalogued, regarding the 78 documented studies, which are fundamental to UAS-based archaeological remote-sensing applications. These parameters for every study were: publication title, year, number of citations, thematic category, number of sensors by type, total number of sensors, sensor brand and model, number of platforms, platform type, platform brand and model, autopilot model, navigation system, flight planning software, type of processing results, spatial resolution of data, complementary terrestrial aerial or satellite sensing techniques used, and study area location. After documenting the significant parameters for each study in a spreadsheet, we performed in-depth data cleaning and confirmed the values of the designated parameters to guarantee data quality and correctness. We performed exploratory analyses using column plots to determine if any trends were evident, regarding UAS-based data acquisitions and processing workflows, in archaeological remote sensing. We were primarily interested in determining the correlations between platforms, sensors, typologies of archaeological terrain, application scenarios, and categories of results obtained.

3.3. State-of-the-Art Survey

In addition to the meta-analysis, we performed a survey of the state-of-the-art of standalone sensors, integrated payloads, and ready-to-fly UAS, available at the time of our review, purposed for archaeological remote-sensing surveys. We also included integrated aerial systems manufactured for other applications—mainly for precision agriculture and infrastructure inspection/monitoring—which can adequately be used for the topics discussed in this paper without additional modifications.

4. Meta-Analysis Results and Discussion

The 68 identified publications [49–116] related to UAS-based archaeological remote sensing, were published between 2012 and 18 June 2020 in 36 different publications/journals. Collectively the International Society of Photogrammetry and Remote Sensing has published 9 articles (~13.2% of the total number of analyzed publications), under the *International Archives of the Photogrammetry,*

Remote Sensing and Spatial Information Sciences, *ISPRS Annals of Photogrammetry, Remote Sensing and Spatial Information Sciences*, and *ISPRS International Journal of Geo-Information*. The WILEY journal *Archaeological Prospection* published the largest number of articles (8), while Elsevier's *Journal of Archaeological Science: Reports* published 5 and MDPI's *Remote Sensing* published 4. The trend in publication had increased each year steadily, until 2018, with the maximum growth in the number of articles published observed between 2017 and 2018 (Figure 1). Citation information derived from Google Scholar shows that the average number of times each publication has been cited is 9.2, with a minimum of 0, a maximum of 84 ([55] published in *Journal of Archaeological Science*), and a median of 3. Archaeological prospection related applications accounted for ~77% of the documented studies, while much smaller numbers were observed for the other types of applications, ~23% for historical terrain visualization, ~13% for archaeogeography, and ~6% for site monitoring applications (Figure 2). Nevertheless, the studies included in the meta-analysis covered a wide range of archaeological contexts and, broad geographic extent.

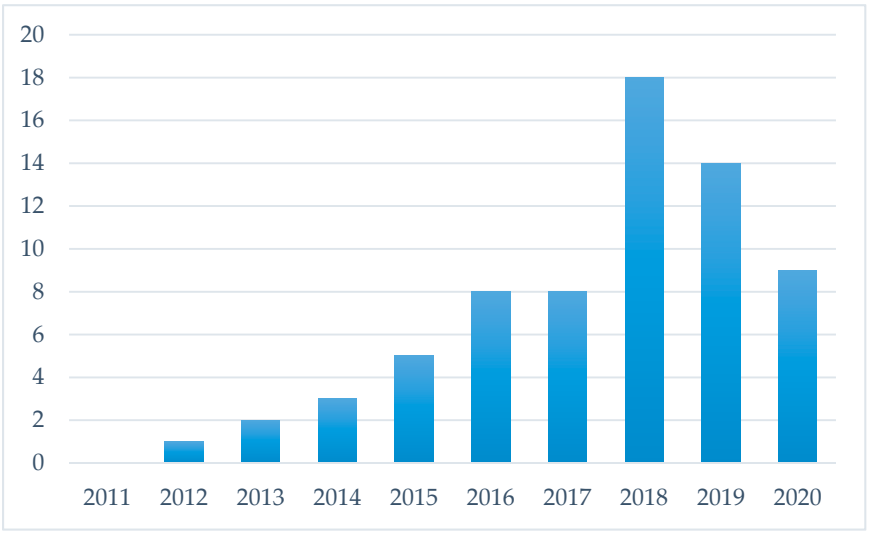

Figure 1. Number of scholarly works related to unmanned aircraft systems (UAS)-based archaeological remote sensing.

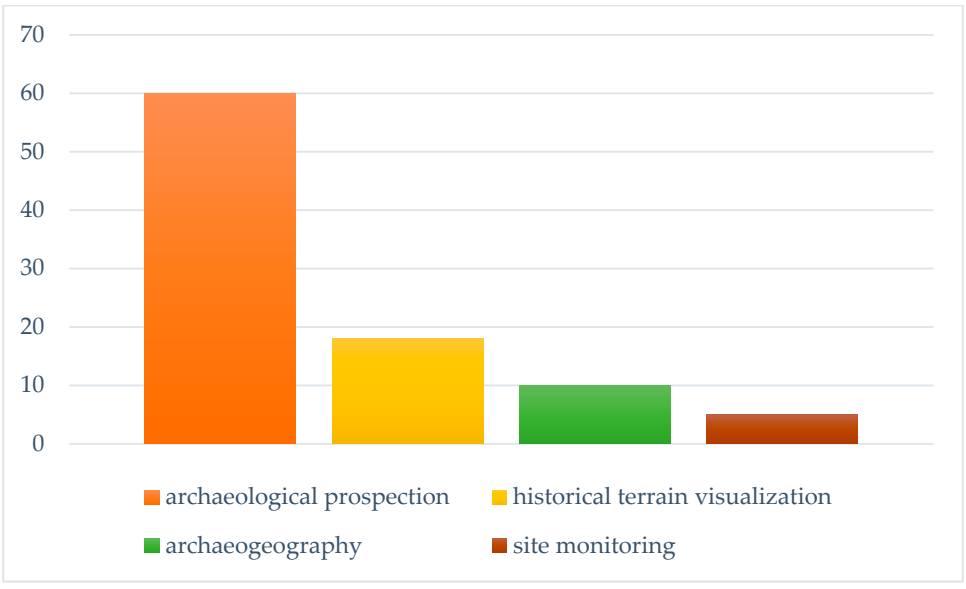

Figure 2. Number of scholarly works related to UAS-based archaeological remote sensing by topic.

Study locations were mapped from the 68 publications, and it was found that UAS have been employed in applied archaeological remote sensing across the world with primary clusters of activity in Europe and North America (Figure 3). A secondary cluster was observed around the tropical countries of Central and South America where dense canopy is obscuring the rich archaeological landscapes and, therefore, increasingly more studies are taking place to reveal and to visualize the hidden historical terrains. Italy leads the ranking of countries where UAS-based archaeological studies have taken place (12), followed by Spain (7), the United States of America (7), Czech Republic (6), the United Kingdom (6), and Greece (4).

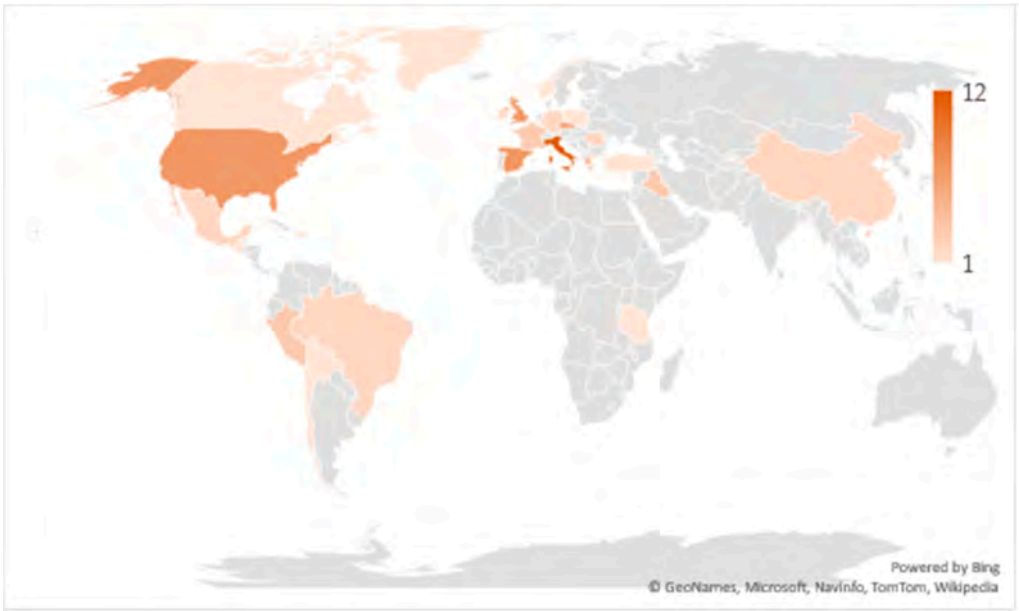

Figure 3. Global distribution of archaeological study sites mapped from information provided in the 75 studies analyzed during the in-depth content analysis.

4.1. Platforms

The majority of studies (60) reported using multirotor-style platforms, which can be attributed to easier maneuverability, higher stability, and the capacity to carry heavier payloads with smaller platform size-to-payload ratios. Only 27 studies reported the use of fixed-wing platforms. In total, 91 platforms were involved in the studies, of which 27 were fixed-wing, 42 quadcopters, 12 hexacopters, and 14 octocopters (circle-shaped, v-shaped, and X8 rotor configurations). The most commonly used platform (Figure 4) was the senseFly eBee, a fixed-wing platform which can be purchased around $25,000 USD with real-time kinematic (RTK) positioning enabled and a SODA 20 MP RGB camera, has a maximum flight time of 50 m, 33 km flight range and optional multi-spectral and thermal sensors available. Other popular choices included the DJI Phantoms and the (discontinued) 3DR SOLO. A few studies reported the use of a custom made platform.

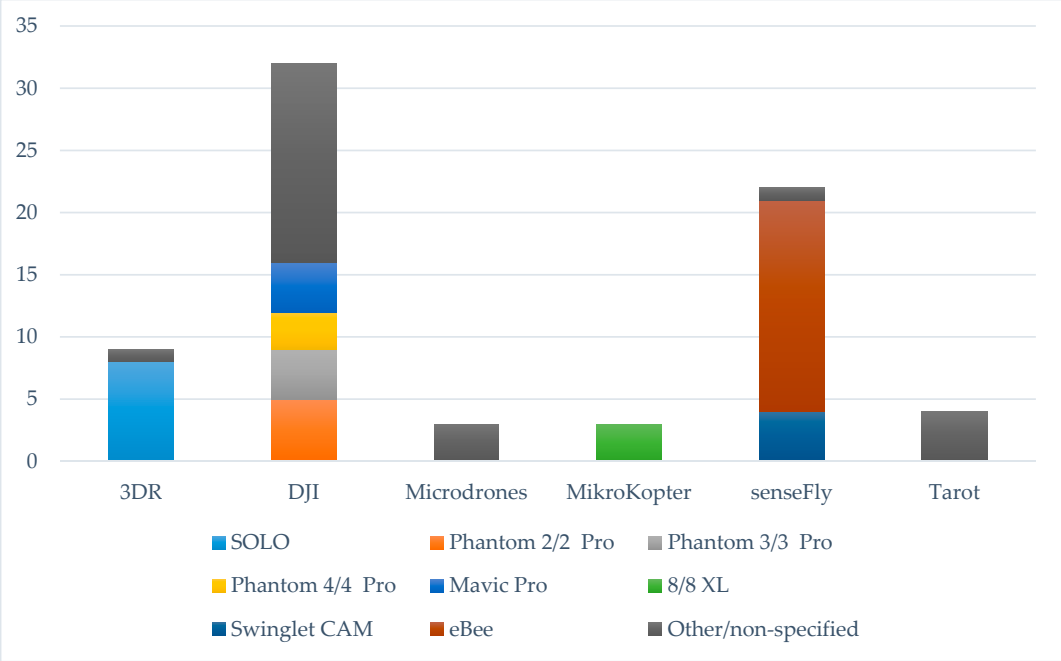

Figure 4. Number of used UAS platforms by manufacturer and model.

4.2. Navigation

A high percentage of the UAS (at least 70%) used for the analyzed studies, and specifically those manufactured by DJI, Microdrones, and senseFly, were ready-to-fly and, therefore, pre-equipped with an autopilot system for navigation control. Of the studies using not ready-to-fly UAS systems, only a few reported the utilized model of autopilot, with Ardupilot APM, Pixhawk, DJI Naza, and the MikroKopter Flight-Ctrl series appearing more often. Similarly, regarding on-platform hybrid measurement units/hybrid navigation system (HMU/HNS), most platforms were already pre-equipped, and only 2 of the studies utilizing non-pre-integrated navigation units [110,112] reported which models were involved; namely an Applanix APX-15 and a NovAtel SPAN-IGM-S1. Most studies (55) reported the use of flight planning software, and only 5 reported performing manual flights, while for the majority of the rest of the studies—that did not report about this matter—it was assumed that flight planning software was used, according to the description of the acquired datasets. The MikroKopter Tool, Pix4Dcapture app, senseFly eMotion, and the free, open-source ArduPilot Mission Planner were the ones encountered more often.

4.3. Sensors

Significantly, 56 studies reported the utilization of multiple sensors, and 12 studies also reported employing multiple platforms (Figure 5). Ten studies used LiDAR sensors, 22 studies used near-infrared (NIR) cameras, 31 studies used thermal-infrared (TIR) cameras, 26 used multi-spectral cameras (MS), and a single study used a hyperspectral (HS) camera (Figure 6). Studies overwhelmingly used pre-equipped or off-the-shelf red, green and blue (RGB) cameras (77%), mainly in combination with other sensors. Canon cameras were a popular choice (used for 31% of the total studies), as 17 studies used Canon off-the-self cameras for RGB acquisition, while 16 studies used Canon cameras for NIR acquisition after they were subjected to a modification in order to be sensitive only in a portion of the NIR spectrum.

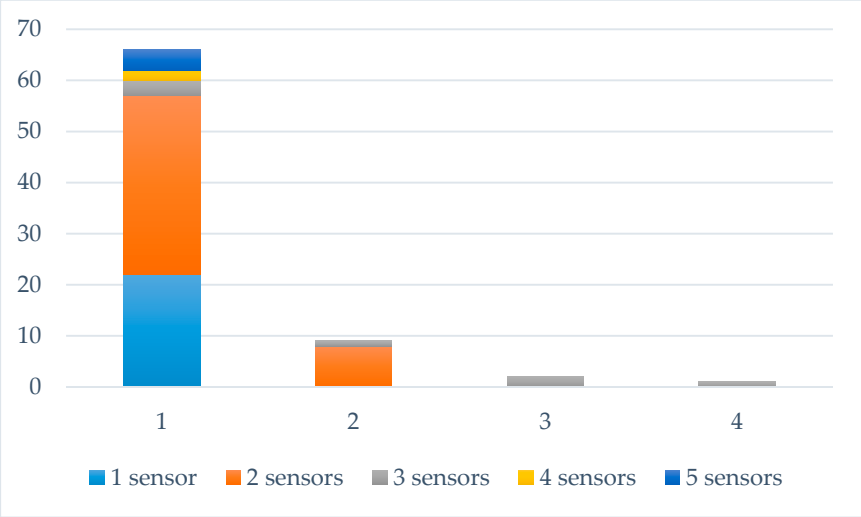

Figure 5. Reported multitude of platforms in the analyzed studies.

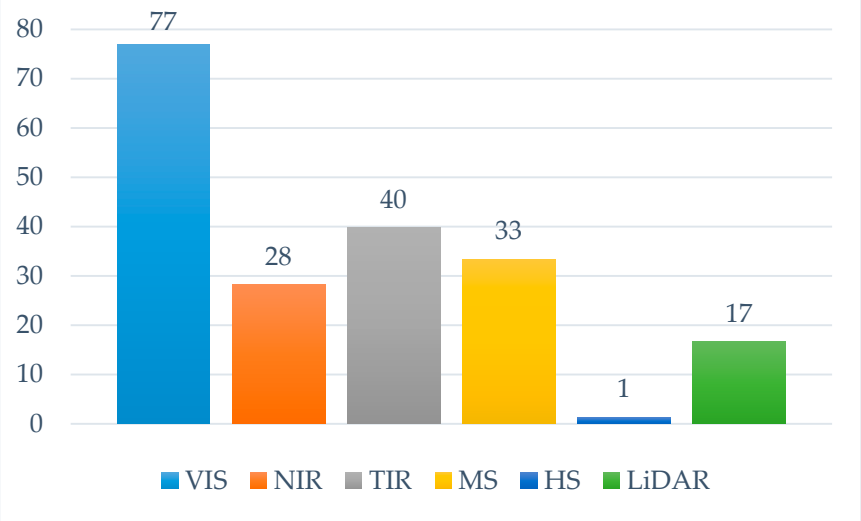

Figure 6. Reported number of sensors by type.

All reported NIR data acquisitions were performed with commercial digital cameras (digital-single-reflex, compact, and action cameras), modified by either the manufacturer of the UAS platform or the researchers. Canon PowerShot ELPH 110HS, PowerShot ELPH 300HS, and PowerShot ELPH S110 were the most frequently used cameras modified for NIR imaging (Figure 7–left). The most recurrently used MS camera was the Parrot Sequoia (11 studies), whereas modified Canon cameras were used in 9 studies, the AIRINOV Multispec4C was used in 5 studies, and the Tetracam ADC Mini-MCA and the MAPIR Survey2 cameras were each reportedly used once (Figure 7–right). Regarding TIR sensors, 16 FLIR-manufactured cameras purposed for UAS integration were reported, but the senseFly thermoMAP was the most popular thermo-camera solution (Figure 8). Most studies captured imagery with nadir—or near nadir—facing cameras; only a handful of studies stated they captured oblique imagery.

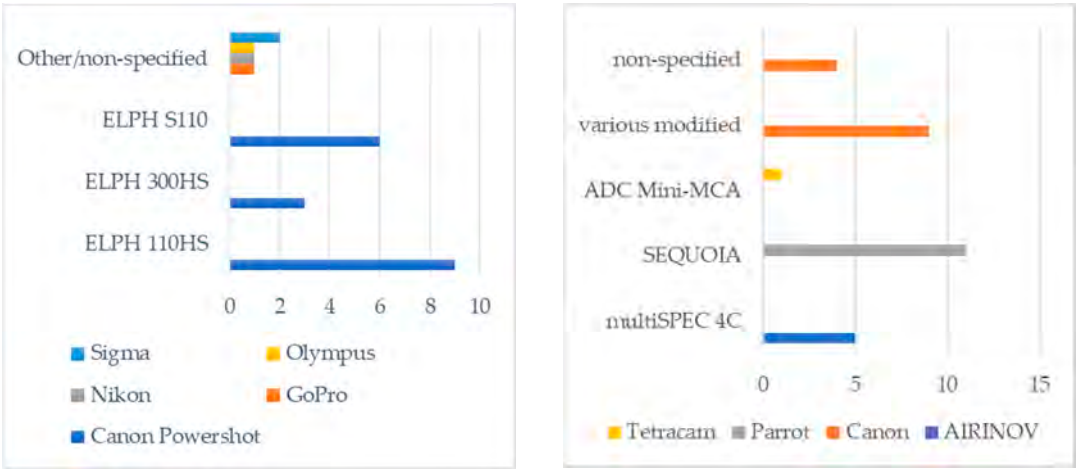

Figure 7. Reported number of near-infrared (NIR, **left**) and multi-spectral (MS, **right**) cameras by manufacturer and model.

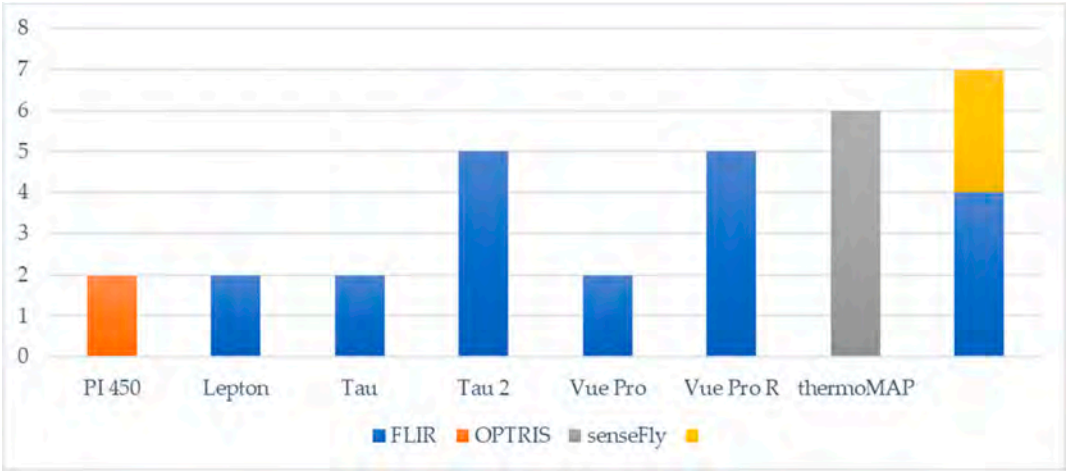

Figure 8. Reported number of thermal-infrared (TIR) cameras by manufacturer and model.

Amongst the miniaturized LiDAR solutions, the Riegl VUX-1UAV and Velodyne VLP-16 were the most used, each having been utilized three times. Furthermore, the Riegl miniVUX-1UAV, the Sparkfunk LiDAR-Lite V2, and the Yellowscan Mapper were used once, while there were also two unreported LiDAR sensors involved in the recorded studies.

4.4. Data Products and Applications

A major part of the recorded UAS-based archaeological prospection activities involved the interpretation of visible spectrum orthophotos/orthophoto-mosaics (68%) and DSMs (55%; for relative percentages see Figure 9), which were mainly produced using structure-from-motion (SfM) and multiple-view-stereo (MVS) approaches. The level of involvement of these products in archaeology can be explained by the high level of automation achieved in the last years, which allows almost automated mapping workflows—from acquisition to analysis of mapping results—for archaeological applications. Flight planning, pre-processing of the images, image-based modeling, production of digital elevation models (DEMs), production of visible, thermal and index maps, and point cloud and image classifications can be realized using the same workstation and software, with minimal interventions, even in real-time. Studies overwhelmingly utilized the Pix4D software platform as an integrated solution to capture imagery datasets (through the mobile application) and create digital models or orthoimages for classification and analysis. Agisoft PhotoScan/Metashape and ArcGIS have also been implemented in a handful of studies for the digitization and analysis procedures,

respectively. Visible orthoimages were commonly exploited towards the manual identification of crop-marks and the integration with results acquired from other spectra to acquire false-color composites. Brooke and Clutterbuck [52] reported an innovative image-enhancing approach using visible spectrum orthophotos; they used Wallis color filtering to increase local contrasts between buried masonry and grass. Additionally, Masini et al. [81] performed multi-temporal investigations to compare negative cropmarks, positive cropmarks, grass marks, and damp marks caused by buried remains. DSMs were interpreted without additional processing in many studies. However, De Reu et al. [72] and Šedina et al. [101] used multitemporal DSMs to construct differential digital surface models (DDSMs), and monitor change over excavated archaeological sites and crop marks, respectively. Several studies exploited the DSM products for interpretative mapping of the archaeological features through PCA and artificial shading [61,63,72,79,88,89,96,97,100,101].

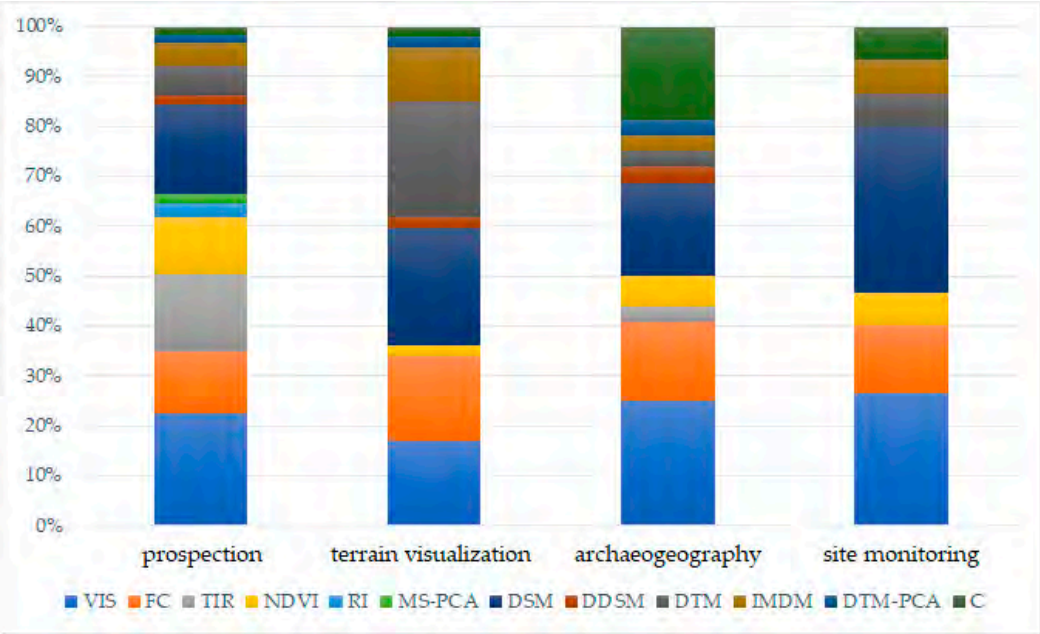

Figure 9. Relative percentages of data products used per application category (VIS—visible orthophoto map; FC—false-color orthophoto map; TIR—thermal infrared orthophoto map; NDVI—normalized difference vegetation index; RI—multiple vegetation and soil reflectance indices; MS-PCA—principal component analysis of multi-spectral imagery products; DSM—digital surface model; DDSM—differential digital surface model; DTM—digital terrain model; IMDM—interpretative mapping of digital models; DTM-PCA—principal component analysis of digital terrain model; C—classification of images, rectified images or ortho-mosaics).

False-color and TIR-orthoimages appeared often in prospections studies (37%, and 47% of the prospection studies respectively). False-color multichannel composites were produced either by using the MS datasets for image-based modeling directly or by combining overlapping orthoimages of different wavelengths. Most MS composites where either reduced through PCA [50,84,109] or processed for normalized difference vegetation index (NDVI) mapping [50,52,54,56,57,60,66–68,70–72,75,76,84–86,97,99,104,109], in order to enhance the contrast between the proxies of buried remains and the landscape matrix. It is worth mentioning that a few studies [50,60,75,86,97,99] reported the use of multiple radiometric vegetation and soil indices to identify which wavelength combinations maximized the local contrasts. Another notable finding was that all thermal investigations were purposed towards archaeological prospection activities. Multi-temporal thermal acquisitions often appeared in the analyzed studies. At the same time, McLeester et al. [84] also pointed out how thermal orthoimages have to be corrected through several steps—from stripping caused by the TIR camera's periodic self-calibration and the thermal

sensor's temperature variations during acquisition—to accurately extract temperature information. Lastly, few prospection studies also reported the use of DTMs to identify topographic reliefs caused by buried historical remains [58,59,73,93,96,98,112]

Activities referring to the accurate visualization of archaeologically rich terrain with UAS-assisted approaches have either explored the use of DSMs or DTMs. While DSMs have been mainly produced with SfM/MVS image-based approaches, DTMs of vegetated areas have been exclusively produced with miniaturized LiDAR sensors [87,96,98,110] or by filtering 3D point clouds derived from image-based modeling with NIR imagery datasets, before constructing the terrain model [49,106]. To a lesser extent, the visualization of historical terrains towards the better interpretation of historical landscapes has been explored in the bibliography by interpretative mapping techniques [65,88,96,100].

In UAS-based archaeogeography applications, the rectified images, ortho-mosaics and raster elevation images have been used in a great extent, and analyzed through classification and shape analysis techniques, to interpret the shape of historical structures [110], the distribution of historical [69] and traditional structures [78], buried remains [77,85], and archaeological artifacts [74,114,116].

Lastly, five applications relevant to UAS-based site monitoring and landscape archaeology have been recorded, most reporting the use of MS data acquisitions. Fenger-Nielsen et al. [64] used NIR intensities detected with a Parrot Sequoia, in combination with soil-content data from site-sampling and satellite imagery, to study the distinct spectral characteristics of vegetation within archaeological sites in Greenland, which showed great potential for archaeological investigations in the Arctic. Khan et al. [73] exploited terrain data obtained with the survey-grade VUX1–UAV LiDAR and two MS cameras, and integrated them with in situ collected archaeological, archaeobotanical, paleo-ecological, and soil data to investigate the scale and nature of the impact of pre-Columbian humans in transforming the Amazonian rainforest landscapes. Mather et al. [82] performed classifications on RGB and NIR imagery data captured with different UAS, and then overlaid—also UAS-captured—topographic data in order to understand the origin of relict landform features. Sonnemann et al. [113] overlaid orthomosaics produced with UAS imagery on high-resolution LiDAR-derived DEM to investigate the topography of pre-colonial settlements in the Caribbean.

5. State-of-the-Art

Overall, the significant developments in unmanned navigation, drone platform manufacturing, integrated sensor miniaturization, and mapping software that have taken place over the last decade, established UAS-based approaches as a significant part of photogrammetry and remote sensing [117]. Benefiting from the above, archaeological science has taken one step forward into embracing these new technologies, through various applications—as discussed earlier. Archaeological low-altitude sensing has substantially evolved from the use of platforms purposed for recreational and photographic uses. It has not only engulfed the advancements of those sensors and integrated systems specifically oriented towards archaeological applications but has also benefited from the progress in other fields, for example, precision agriculture and monitoring of structures, who profit from similar UAS-borne sensing. Recent archaeological studies expand the scientific horizons beyond the visual interpretation of the data products and discuss how previously invisible and undocumented features are revealed, while simultaneously paying attention to the spatial and radiometric accuracy and precision of presented results. It goes without saying that high-resolution and high-accuracy products, and information retrieval from multiple wavelengths, are accompanied by considerable costs. Although a trend is evident regarding researchers who invest in high-end fully autonomous integrated UAS, more application-oriented projects seem to prefer custom solutions. Therefore, in this section, we provide information on both integrated ready-to-fly UAS and specialized options for payload integration. Table 1 provides some examples of integrated solutions, which are purposed or can be repurposed for archaeological remote sensing surveys (also examples in Figure 10). The reported integrated systems are ready-to-fly UAS with pre-equipped navigation system, autopilot, sensors, gimbals, and all necessary electrical on-board equipment.

Table 1. Examples of integrated ready-to-fly UAS which can be used for archeological surveys.

Brand	Model	Platform Type	Sensors	Max. Flight Time (m)
DJI	P4 Multispectral	quad-copter	RGB + 5 monochrome multispectral	27
	Matrice 200 V2	quad-copter	FPV RGB cameras *, RGB cameras *, Zenmuse XT	24
	Matrice 600 PRO	hexa-copter	FPV RGB cameras *, RGB cameras *, Zenmuse XT	16–18
Intel	Falcon 8+	octo-copter	Panasonic ZS50 RGB camera + Flir Tau 2 640	16–26
	Sirius Pro	fixed-wing	Sony a6300 *, RX1R II *, MicaSense RedEdge *	
Leica	Aibot AX20	quad-copter	Sony α6300/Sony α7RII	24
Microdrones	mdLiDAR3000LR aaS	quad-copter	Riegl VUX-1UAV	27–32
	mdLiDAR3000 aaS	quad-copter	Riegl miniVUX-2UAV + Sony RX1R II	27–32
	mdLiDAR1000 aaS	quad-copter	SICK LD-MRS4 LiDAR + FLIR 5MP Global Shutter	25
Parrot	Bluegrass Fields	quad-copter	Parrot Sequoia	25
	ANAFI Thermal	quad-copter	FLIR Lepton 3.5	26
Riegl	RiCOPTER with VUX-SYS	quad-copter	VUX-1UAV, up to 3 high-resolution cameras *	30
senseFly	eBee X	fixed-wing	senseFly Duet T *, Parrot Sequoia+ *	90
QuestUAV	DATAhawk ^{AG}	fixed-wing	MicaSense RedEdge	55

Note: RGB: Red Green Blue; FPV: First-person view; * Option provided by the manufacturer.

Figure 10. Examples of integrated ready-to-fly UAS: (**A**) DJI P4 Multispectral; (**B**) Intel Falcon 8+; (**C**) Leica Aibot AX20; (**D**) Microdrones mdLiDAR1000 aaS; (**E**) Intel Sirius Pro; (**F**) Parrot ANAFI Thermal; (**G**) senseFly eBeeX; (**H**) QuestUAV DATAhawk ^{AG}.

5.1. Platforms

UAS operated for archaeological remote sensing mainly fall into the *Micro* (<2 kg weight, up to 200 m altitude, <5 km radius, <1 h endurance), *Mini* (2–20 kg weight, up to 3000 m altitude, <25 km radius, 1–2 h endurance), and seldom *Small* (20–150 kg weight, up to 5000 m altitude, <50 km radius, 1–5 h endurance) categories (after Qi et al. [118]). While the quality of acquired datasets depends largely on on-board sensors (described in Sections 5.4–5.7), platform typology and configuration play an essential role in the success of the remote-sensing mission, simultaneously constraining the payload that may be deployed and the flight planning. Fixed-wing UAS have a clear advantage

in archaeological surveys because their longer flight autonomy allows the coverage of much more extensive historical sites and landscapes than the average multi-rotor (Table 2). Fixed-wing aircrafts' increased stability allows greater control over flight parameters and the quality of collected data. However, the competition with rotary-wing aircraft is always present because multi-rotors have greater maneuverability and allow heavier payloads and more customizability, therefore having more options for sensor integration.

Table 2. Comparison between different features of fixed-wing and multi-rotor UAS, modified from Jeziorska [119].

	Fixed-Wing	**Multi-Rotor**
Advantages	long flight autonomy better control of flight parameters higher control of data quality greater stability higher flight safety	greater maneuverability more compact and portable easy to use higher payload capacity more flexibility in payload configuration ability to hover small landing/take-off zone
Disadvantages	less compact and portable challenging to fly larger take-off/landing site needed	shorter range less stable in the wind

Multi-rotor UAS are additionally more compact (speaking for the same platform body size-to-payload weight ratio), and subsequently more easily transportable. Despite their short flying duration, which limits the archaeological area that can be covered within a single flight, they have some distinct attributes that may be necessary in certain contexts, as the ability to hover and capture data while remaining over one place, the ease of capturing oblique imagery, and vertical take-off and landing that allows for more flexible deployment in areas that would be inaccessible with fixed-wing aircraft. Some conventional multi-rotor frames used in customized UAS for archaeological applications are MikroKopter's MK8-2500 (8 rotors, folded dimensions 64 cm × 60 cm, max. payload 2.5 kg) and MK8-3500 (8 rotors, max. payload 3.5 kg), and VulcanUAV's Black Widow (4 rotors, max payload 4.6 kg) and Raven (8 rotors-X8 configuration, max. payload 10 kg).

5.2. Orientation Systems

The miniaturization of computer boards, Global Navigation Satellite Systems (GNSS) receivers and antennas, inertial measurement units (IMUs) and, in general, electronics has allowed the integration of hybrid measurement units (HMU) for UAS whose measurements can be processed, in a hybrid navigation system (HNS) or in post-processing, in a hybrid orientation system (HOS). The results depend on the quality of the GNSS receiver and the GNSS antenna, and the accuracy of the attitude part of the orientation is highly dependent on the IMU quality and flight dynamics. To deliver orientation parameters, and data products at cm-level with increased reliability, primarily two modifications of kinematic GNSS measurements are being adopted for UAS applications. RTK—which considers that there is real time communication of the UAS with a ground reference station (using radio link)—delivers corrections to GNSS measurements during the flight. Post-processed kinematic (PPK), on the other hand, depends on corrections from a reference station that are applied post-flight [120,121]. As RTK-enabled receivers have already been available on several commercial platforms, and PPK is becoming more common for UAS-based archaeological surveys, it is useful to review the current capabilities of HMU and HNS solutions for unmanned aircraft operations. Therefore, the state-of-the-art integrated solutions are presented in Table 3, taking into consideration that the values given are simply indicative as they include general specifications and optimal testing conditions.

Table 3. Commercial hybrid measurement units and hybrid navigation systems for unmanned aerial orientations.

Make	Model	Weight (kg)	GNSS Φ or ρ	$\sigma_{p\ hz}$ SPS (m)	$\sigma_{p\ hz}$ RTK (m)	$\sigma_{p\ hz}$ RTK* (m)	σ_{α} (μG/$\sqrt{Hz}$)	σ_{ω} (deg/s/$\sqrt{Hz}$)	$\sigma_{\theta,\gamma}$	σ_{ψ}
Trimble	APX-20 UAV	420	Φ	1.5–3.0	0.02–0.05	0.02–0.05	NA	NA	0.015	0.035
iMAR	iNAT-M200-FLAT/SLN	550	Φ	0.4–1.8	0.1	0.03	60	0.150	0.030	0.100
iMAR	iNAT-M200/MLN	900	Φ	0.4–1.8	0.1	0.03	25	0.150	0.010	0.030
Adv. Nav.	Spatial-Dual	304	ρ	0.5–1.2	NA	0.008	100	0.004	0.030	0.060
NovAtel	SPAN CPT7	495	Φ	1.0	0.02	0.01	NA	NA	0.005	0.010

Note: Φ: phase measurements; ρ: code measurements; $\sigma_{p\ hz}$: horizontal position accuracy (RMS); SPS: standard positioning service; RTK: real-time kinematic; RTK*: real-time kinematic post-processed; σ_{α}: linear accelerations' noise (PSD level); σ_{ω}: angular rates' noise (PSD level); $\sigma_{\theta,\gamma}$: roll and pitch precision (whole spectrum); σ_{ψ}: heading precision (whole spectrum); NA: not available.

5.3. Light Detection and Ranging (LiDAR) Sensors

The reduction in LiDAR sensor size and price are making them more common for UAS-based archaeological surveys. The market of 3D laser scanners for unmanned platforms has grown rapidly, and the technological developments are increasing the quality of data acquired by these sensors. This creates the prospect of replacing airborne LiDAR since essential characteristics of LiDAR data are largely unaffected by the carrying platform, which implies that existing well-developed processing techniques can be used on these data. Limitations caused by the tradeoff between performance and size or cost of LiDAR, can be partially overcome by the proximity of the sensor and the surveyed area in comparison to airborne scanning. Presently Quanergy, Riegl, and Velodyne dominate the market of LiDAR sensors manufactured to be mounted on UAS (examples in Figure 11), as the overwhelming majority of integrated payload for scanning, include their products. Table 4 presents the available lightweight LiDAR sensors. A detailed account of integrated LiDAR payloads can be found in Appendix A.

Figure 11. Examples of LiDAR sensors for UAS: (**A**) RIEGL VUX-1UAV; (**B**) RIEGL miniVUX-2UAV; (**C**) Velodyne HDL-32E; (**D**) Velodyne Puck 32MR; (**E**) Quanergy M8-Core; (**F**) Quanergy M8-PoE+.

Table 4. Light detection and ranging (LiDAR) sensors for UAS.

Make	Model	Range (m)	FOV (deg)	Max. Returns	Shots/s (1000) *	Accuracy (cm)	Weight (kg)
Quanergy	M8-Core	100	(V) 20, (H) 360	3	430	3	0.90
	M8-Plus	150	(V) 20, (H) 360	3	430	3	0.90
	M8-Ultra	200	(V) 20, (H) 360	3	430	3	0.90
	M8-PoE+	150	(V) 20, (H) 360	3	430	3	1.36
RIEGL	VUX-1UAV	340	330	4	550	1	3.5
	miniVUX-1UAV	330	360	5	100	1.5	1.6
	miniVUX-2UAV	280	360	5	200	1.5	1.6
	miniVUX-1DL	260	(C) 46	5	100	1.5	2.5
Velodyne	HDL-32E	100	(V) 41.33, (H) 360	2	695	2	1.0
	Puck	100	(V) 30, (H) 360	2	300	3	0.83
	Puck LITE	100	(V) 30, (H) 360	2	300	3	0.59
	Puck 32MR	120	(V) 40, (H) 360	2	600	3	0.93
	Ultra Puck	200	(V) 40, (H) 360	2	600	3	0.93

Note: FOV: field-of-view; (V) vertical; (H) horizontal; (C) circular; * at maximum laser pulse repetition rate (PRR) and full power—single return.

5.4. Near-Infrared and Multi-Spectral Cameras

The exploitation of NIR imagery can contribute significantly to UAS-based archaeology [122], and therefore various sensor solutions have been explored to incorporate the NIR spectrum in prospection-related applications. As the meta-analysis revealed, the Canon S110 digital cameras, modified for red-edge and near-infrared imaging, have been frequently used over the past decade, serving as a default multi-spectral solution for the senseFly fixed-wing aircrafts until 2014. These cameras are currently being replaced by various high-resolution models, as the modification of compact and digital single-lens reflex (DSLR) cameras, for beyond-visible acquisition, becomes more prevalent. At the same time, various lower-resolution lightweight camera options for UAS-based MS imaging are available, having the advantage of more than three narrower bands. Table 5 summarizes the characteristics of some typical and/or representative camera options (in Figure 12).

Table 5. Multi-spectral cameras for UAS.

Brand	Model	System Configuration	Multi-Spectral Bands	Single-Band Resolution (px)
Buzzard	Six Band	6-camera	B, G, R, NIR1, NIR2, NIR3	1280 × 1024
MicaSense	RedEdge-MX	5-camera	B, G, R, RE, NIR	1280 × 960
	Altum	5-camera + LWIR camera	B, G, R, RE, NIR, LWIR	2064 × 1544
Parrot	Sequoia+	4-camera + RGB camera	G, R, RE, NIR	1280 × 960
SAL	MAIA WV	9-camera	VIS, V, B, G, R, RE, NIR1, NIR 2	1280 × 960
Tetracam	MCAW	6-camera (450–1000 nm)	user-selectable	1280 × 1024
	Micro-MCA	4, 6 or 12-camera	user-selectable	1280 × 1024
	RGB + 3	4-camera	VIS, NDVI R + RE + NIR	1280 × 1024
	ADC-Micro	single 3-band camera	G, R, NIR	2048 × 1536

Note: B: blue; G: green; R: red; NIR: near-infrared; RE: red-edge; LWIR: long-wave infrared.

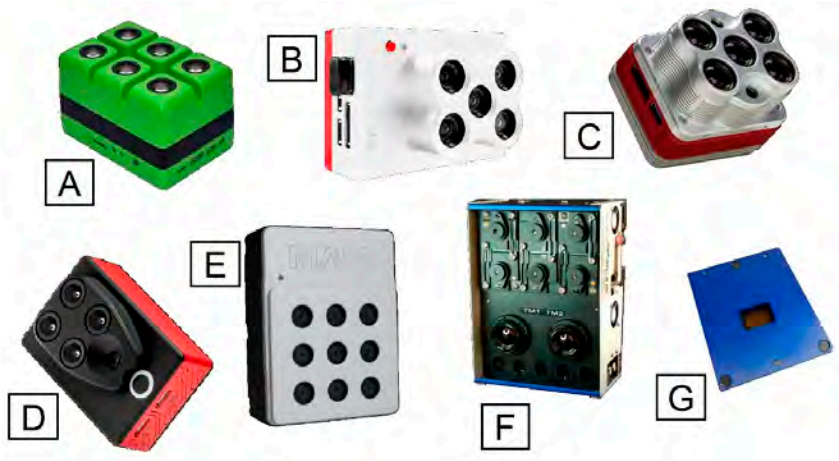

Figure 12. Examples of multi-spectral cameras for UAS: (**A**) Buzzard Six Band; (**B**) MicaSense RedEdge-MX; (**C**) MicaSense Altum; (**D**) Parrot Sequoia+; (**E**) SAL MAIA WV; (**F**) Tetracam MCAW; (**G**) Tetracam ADC-Micro.

5.5. Hyperspectral Cameras

To cover the need for the detection of information from multiple very narrow bands of the electromagnetic spectrum [123], and towards the more accurate calculation of vegetation and soil indices, HS imaging sensors have consistently been miniaturized, and can currently be mounted on UAS platforms. Some of them are listed in Table 6 (also examples in Figure 13). It is the authors' opinion that these sensors will continue to play a significant role in UAS-based archaeological prospection, and geoarchaeology.

Table 6. Hyperspectral cameras for UAS (weight ≤ 2 kg).

Brand	Model	Spectral Range (nm)	Bands	Spectral Step (nm)	Resolution (px)	Acquisition Mode	Weight (kg)
BaySpec	OCI-UAV-D1000	450–970	120	5.0 [a]	2000	P	1.14
Brandywine Photonics	CHAI V-640	400–1000	256	2.5, 5.0, 10.0	640 × 512	S	0.48 [d]
Corning Inc.	vis-NIR microHSI	400–800 400–1000 380–880	120 180 150	3.3 [a]	1360 [c]	P	0.45
	vis-SWIR	600–1700	110	10.0 [a]	1280 [c]	P	1.6
	SWIR microHSI 640C	850–1700	170	5.0 [a]	640 [c]	P	1.1
	alpha-SWIR microHSI	900–1700	160	5.0 [a]	640 [c]	P	1.2
	LWIR	7800–13,400	60	100 [a]	320 [c]	P	1.15
Headwall Photonics Inc.	Nano-Hyperspec	400–1000	270	6 [a]	640 [c]	P	0.5 [d]
	Micro-Hyperspec	400–1000	324/369	5.8/5.8 [a]	1004/1600 [c]	P	0.7/1.1 [d]
		900–1700	134/67	10.0/10.0 [a]	640/320 [c]		0.9 [d]
		600–1700	267	5.5 [a]	640 [c]		0.9 [d]
		900–2500	166/267	10/8 [a]	384/640 [c]		2.0/1.6 [d]
Photonfocus	MV1-D2048 × 1088-HS05-G2	470–900	150	10.0 [b]	2048 × 1088	S	0.265 [d]
RESONON	Pika L	400–1000	281	2.1 [b]	900 [c]	P	0.6
SENOP	HSC-2.1-B HSC-2.1-C	450–800 500–900	≤1000	1.0 [a]	1024 × 1024	S	0.99
SPECIM	FX10	400–1000 400–780	224	5.5 [a]	1025 × 1024	S	1.3
	FX17	900–1700	224	8.0 [a]	640 × 640	S	1.56
XIMEA	MQ022HG-IM-LS100-NIR	600–1000	100	4.0 [b]	2048 × 1088	S	0.032 [d]
	MQ022HG-IM-LS150-VISNIR	470–900	150	3.0 [b]			
	MQ022HG-IM-SM4X4-VIS	470–620	16	10.0 [b]			
	MQ022HG-IM-SM5X5-NIR	665–975	25	12.5 [b]			
	MQ022HG-IM-SM4X4-REDNIR	630–780	16	10.0 [b]			

Note: [a] at FWHM; [b] by sampling; [c] pushbroom line length (the other dimension depends on sensor's sweep distance); [d] without lens, inertial navigation and global navigation satellite systems; P—pushbroom; S—snapshot.

Figure 13. Examples of hyperspectral cameras for UAS: (**A**) Photonfocus MV1-D2048x1088-HS05-G2; (**B**) RESONON Pika L; (**C**) SENOP HSC-2; (**D**) SPECIM FX10; (**E**) XIMEA xiSpec Series.

5.6. Thermal Cameras

There have been essential advancements in thermal camera miniaturization in recent years. Lightweight, small-size LWIR imagers, such as those developed by FLIR, were first introduced in a military context for remote reconnaissance and are becoming more common in UAS-based remote-sensing applications such as archaeological prospection. Table 7 compiles some existing products in the family of thermal sensors, suitable for light UAS (also examples in Figure 14).

Table 7. Thermal cameras for UAS.

Manufacturer	Model	Spectral Range (μm)	Resolution (px)	Pixel Size (μm)	Accuracy (±°C)	Weight (g)
FLIR	Lepton 3.5	8–14	160 × 120	12	5	0.9 [b]
	Vue Pro	7.35–13.5	336 × 256	17	5	92–113
	Vue Pro R	7.35–13.5	640 × 512	17	5	92–113
	Zenmuse XT	7.35–13.5	640 × 512 [a]	17	5	270
	Zenmuse XT2	7.5–13.5	640 × 512 [a]	17	5	588
ICI	9320 P-Series	7–14	320 × 240	17	1	37 [b]
	9640 P-Series	7–14	640 × 480	17	1	37 [b]
	SWIR 320 P-Series	7–14	320 × 256	15	1	130 [b]
	SWIR 640 P-Series	7–14	640 × 512	15	1	130 [b]
InfraTec	VarioCAM HDx head S	7.5–14	640 × 480	17	2	1100
Leonardo DRS	TAMARISK Precision320	7.5–14	320 × 240	17	5	48–134
	TAMARISK Precision640	7.5–14	640 × 480	17	5	90–295
	Tenum640	8–14	640 × 512	10		39–48
Optris	PI 450i	8–14	382 × 288	17	2	195
	PI 640	8–14	640 × 480	17	2	320
Thermoteknix	MicroCAM 2	8–12	640 × 480 [a]	17		43 [b]
	MicroCAM 3	8–12	640 × 480 [a]	17		30 [b]
Xenics	Gobi 640-Series	8–14	640 × 480	17		208–263 [b]

Note: [a] maximum resolution configuration; [b] excluding lens.

Figure 14. Examples of thermal cameras for UAS: (**A**) FLIR Vue Pro R; (**B**) ICI 9640 P-Series; (**C**) VarioCAM HDx head S; (**D**) Leonardo DRS TAMARISK Precision; (**E**) Optris PI 640; (**F**) Xenics Gobi 640-Series.

5.7. Ground-Penetrating Radars

A ground-penetrating radar (GPR) is an active non-destructive geophysical sensing technique that utilizes electromagnetic radiation in the microwave band and has always been entangled with archaeological prospection for the subsurface mapping of artifacts, features, and patterning [124,125]. Although there are currently no integrated payload solutions for UAS-borne microwave-based detection, a few recent studies report experiments towards the manufacture of customized systems for GPR non-destructive applications [126–128].

6. Conclusions

The last decade was marked by a radical miniaturization and integration of UAS-mounted sensors, which gradually fostered the adoption of low-altitude sensing techniques for archaeological applications, including but not limited to prospection. Notwithstanding the considerable number of works reviewed here, UAS-based archaeological remote-sensing applications and, especially, those dealing with the beyond-visible spectra to identify multi-spectral contrast variations, are still scarce. This is most likely because the relevant technology has only recently reached a certain level of maturity and high-resolution solutions remain considerably expensive. The recently observed trends, regarding increasingly more metrically and radiometrically accurate data-acquisition and data production in archaeological surveys, and the adoption of well-established processing and analytical techniques from satellite and airborne sensing, suggest a promising perspective. However, the aspects of spatial precision and accuracy still remain undocumented in numerous archaeological surveys which suggests a need for better training regarding metric concepts and for increasing the collaborations between archaeologists and geomatics experts to achieve optimal results in archaeological remote-sensing projects. Metric, radiometric and semantic contents of acquired archaeological data and meta-data should not be neglected as they contain valuable information for archaeological interpretations. It should be further highlighted that automation in the detection of historical residues remains an undeniably complex and challenging task due to the unique morphological, stratigraphical, topographical and archaeological characteristics of each archaeological site [129–131]. For this reason the majority of UAS-borne prospection studies still depend on the parallel acquisition of data with ground-based geophysical methods such as electrical resistivity surveys, ground-penetrating radar, electromagnetic conductivity surveys, and magnetic gradiometry surveys, on historical aerial footage, and on satellite datasets, which complete our

perspectives over historical terrains. Lastly, the authors would like to point out that, despite the observed allocation of the analyzed studies on a global scale, the gaps on the relevant map do not necessarily reflect the contemporary worldwide distribution of archaeological remote-sensing research. There are various reported examples of innovative archaeological studies in Oceania and Asia [132–135]—actively using drones—which due to the strictly set selection criteria were excluded from the presented meta-analysis. The typology of the historical remains also plays a large part in this distribution anomaly. However, UAS-based remote sensing is widely applied in these areas, mainly directed towards heritage recording.

Supplementary Materials: The following is available online at http://www.mdpi.com/2504-446X/4/3/046/s1: Figure S1. PRISMA 2009 flow diagram, Table S2. List of meta-analysis publications.

Author Contributions: Conceptualization, E.A.; Data Curation, E.A.; Methodology, E.A.; Validation, E.A.; Formal analysis, E.A.; Investigation, E.A.; Resources, E.A.; Writing–Original draft, E.A.; Visualization, E.A.; Writing–review and editing, E.A. and F.R., Supervision, F.R.; Project administration, F.R.; Funding acquisition F.R. All authors have read and agreed to the published version of the manuscript.

Funding: This project has received funding from the European Union's Framework Program for Research and Innovation Horizon 2020 (2014–2020) under the Marie-Skłodowska Curie Grant Agreement No. 754511 and from the Compagnia di San Paolo.

Conflicts of Interest: The authors declare no potential conflict of interest.

Abbreviations

3D	Three-Dimensional
DDSM	Differential Digital Surface Models
DEM	Digital Elevation Model
DSLR	Digital Single-Lens Reflex
DSM	Digital Surface Model
DTM	Digital Terrain Model
GIS	Geographic Information Systems
GNSS	Global Navigation Satellite Systems
GPR	Ground-Penetrating Radar
HMU	Hybrid Measurement Units
HNS	Hybrid Navigation System
HOS	Hybrid Orientation System
HS	Hyper-spectral
IMU	Inertial Measurement Units
LiDAR	Light Detection and Ranging
LRM	Local Relief Modeling
LWIR	Long-Wavelength Infrared
MS	Multi-spectral
MVS	Multiple-View-Stereo
NDVI	Normalized Difference Vegetation Index
NIR	Near-Infrared
PCA	Principal Component Analysis
PPK	Post-Processed Kinematic
RGB	Red Green Blue
RPAS	Remotely Piloted Aircraft Systems
RTK	Real-Time Kinematic
SfM	Structure-from-Motion
SPS	Standard Positioning Service
SVF	Sky-View Factor
TIR	Thermal Infrared
UAS	Unmanned Aerial Vehicle
VIS	Visible

Appendix A.

Table A1. Integrated LiDAR payloads for UAS.

Brand	Model	Max. Range (m)	FOV (deg)	Max. Returns	Shots/s (1000) **	Accuracy (cm)	Weight (kg)	LiDAR Sensor	GNSS	IMU	Storage	Camera
3D Target	Scanfly HD2	120	(V)40, (H)360	2	300	5	1.95	Velodyne Puck 32MR	☑	☑	☑	☒ *
	Scanfly LITE	100	(V)30, (H)360	2	300	5	1.6	Velodyne Puck Lite	☑	☑	☑	☒ *
	Scanfly ULTRA		(V)40, (H)360	2	600	5	0.95	Velodyne Ultra Puck	☑	☑	☑	☒ *
Emesent	Hovermap HF1	100	360	2	300	3	1.8	Velodyne VLP-16 Lite	☑	☑	☑	☒
	Hovermap VF1	100	360	2	300	3	1.8	Velodyne VLP-16 Lite	☑	☑	☑	☒
GeoCue Group	True View 410 3DIS	200	(V)20, (H)360	3	430	3	2	Quanergy M8-Ultra	☑	☑	☑	☑
Geodetics	Geo-MMS LiDAR M8	150	(V)20, (H)360	3	430	3		Quanergy M8-Core	☑	☑	☑	☒
	Geo-MMS LiDAR VLP-16	100	360	2	300	5	1.59	Velodyne VLP-16	☑	☑	☑	☒
	Geo-MMS LiDAR VLP-32E	100	(V)40, (H)360	2	700	6		Velodyne VLP-32E	☑	☑	☑	☒
	Geo-MMS LiDAR VLP-32C	200	(V)40, (H)360	2	600	3		Velodyne VLP-32C	☑	☑	☑	☒
	Geo-MMS LiDAR CL-360	775	360	4	310	1		Teledyne Optech CL-360	☑	☑	☑	☒
LiDAR SWISS	LS Nano M8	200	360	3	400	2	1.95	Quanergy M8-Core	☑	☑	☑	☑
	LS Nano Vux	330	360	5	100	5	2.95	RIEGL miniVUX-1UAV	☑	☑	☑	☑
	Surveyor	100	360	2	300	5	2.3	Velodyne VLP-16	☑	☑	☑	☑
	Surveyor Ultra	200	360	2	600	5	2.7	Velodyne VLP-32	☑	☑	☑	☑
LiDARUSA	Revolution 60	100	360	2	300	4.6	1.53	Velodyne PUCK	☑	☑	☑	☑
	M200 Series Snoopy	150	(V)40, (H)360	2	440	2	1.7	Quanergy M8-Core	☑	☑	☑	☑
	Snoopy A-series	100	(V)40, (H)360	2	700	6	2.51	Velodyne VLP-32E	☑	☑	☑	☑
	Snoopy miniVUX	330	360	5	100	5	2.9	RIEGL miniVUX-1UAV	☑	☑	☑	☑
Phoenix	SCOUT-16	100	(V)30, (H)360	2	300	5.5	1.65	Velodyne VLP-16	☑	☑	☑	☒ *
	SCOUT-32	100	(V)41.33, (H)360	2	700	2	2.4		☑	☑	☑	☒ *
	miniRANGER-LITE	250	360	5	100	1.5	1.55	RIEGL miniVUX-1UAV	☑	☑	☑	☒ *

Table A1. *Cont.*

Brand	Model	Max. Range (m)	FOV (deg)	Max. Returns	Shots/s (1000) **	Accuracy (cm)	Weight (kg)	LiDAR Sensor	GNSS	IMU	Storage	Camera
PolyExplore	Polyscanner LM16	100	(V)30, (H)360	2	300	3	2.3	Velodyne VLP-16	☑	☑	☑	☒
	Polyscanner LM32	200	(V)40, (H)360	2	600	3	2.3	Velodyne VLP-32C	☑	☑	☑	☒
	Polyscanner LM16C	100	(V)30, (H)360	2	300	3	2.3	Velodyne VLP-16	☑	☑	☑	☑
	Polyscanner LM32C	200	(V)40, (H)360	2	600	3	2.3	Velodyne VLP-32C	☑	☑	☑	☑
RedTail	RTL-400	120	(V)40, (H)40	5	200	1.5	2.1	OEM	☑	☑	☑	☒
Routescene	LidarPod	100	(V)40, (H)360	2	700	6	1.3	Velodyne VLP-32E	☑	☑	☑	☒
ScanViz	SV-Mini	200	(V)40, (H)360	2	600	2.5	1.4	Velodyne VLP-32C	☑	☑	☑	☑
South	SZT-V100	100	(V)30, (H)360	2	300	3	1.5	Velodyne VLP-16	☑	☑	☒	☒
	SZT-V200	200	(V)40, (H)360	2	600	3	1.6	Velodyne VLP-32	☑	☑	☒	☒
	SZT-R250	250	360	5	100	1.5	2.1	RIEGL miniVUX-1UAV	☑	☑	☑	☒
YellowScan	Surveyor	100	360	2	300	5	1.6	Velodyne VLP-16	☑	☑	☑	☒ *
	Surveyor Ultra	200	360	2	600	5	1.7	Velodyne VLP-32	☑	☑	☑	☒ *
	Vx-15	330	360	5	100	5	2.6	RIEGL miniVUX-1UAV	☑	☑	☑	☒ *
	Vx-15+	330	360	5	200	5	2.6	RIEGL miniVUX-2UAV	☑	☑	☑	☒ *

Note: (V) vertical; (H) horizontal; * optional; ** at maximum laser pulse repetition rate (PRR) and full power—single return.

References

1. Gojda, M. The Contribution of Aerial Archaeology to European Landscape Studies: Past Achievements, Recent Developments and Future Perspectives. *J. Eur. Archaeol.* **1997**, *5*, 91–104. [CrossRef]
2. Bewley, R.H. Aerial survey for archaeology. *Photogramm. Rec.* **2003**, *18*, 273–292. [CrossRef]
3. Ceraudo, G. Aerial Photography in Archaeology. In *Good Practice in Archaeological Diagnostics*; Corsi, C., Slapšak, B., Vermeulen, F., Eds.; Natural Science in Archaeology; Springer International Publishing: Cham, Switzerland, 2013; pp. 11–30. ISBN 978-3-319-01783-9.
4. Ciminale, M.; Becker, H.; Gallo, D. Integrated technologies for archaeological investigation; the Celone Valley project. *Archaeol. Prospect.* **2007**, *14*, 167–181. [CrossRef]
5. Campana, S.; Dabas, M.; Marasco, L.; Piro, S.; Zamuner, D. Integration of remote sensing, geophysical surveys and archaeological excavation for the study of a medieval mound (Tuscany, Italy). *Archaeol. Prospect.* **2009**, *16*, 167–176. [CrossRef]
6. Sarris, A.; Papadopoulos, N.; Agapiou, A.; Salvi, M.C.; Hadjimitsis, D.G.; Parkinson, W.A.; Yerkes, R.W.; Gyucha, A.; Duffy, P.R. Integration of geophysical surveys, ground hyperspectral measurements, aerial and satellite imagery for archaeological prospection of prehistoric sites: The case study of Vésztő-Mágor Tell, Hungary. *J. Archaeol. Sci.* **2013**, *40*, 1454–1470. [CrossRef]
7. Caspari, G.; Sadykov, T.; Blochin, J.; Buess, M.; Nieberle, M.; Balz, T. Integrating Remote Sensing and Geophysics for Exploring Early Nomadic Funerary Architecture in the "Siberian Valley of the Kings". *Sensors* **2019**, *19*, 3074. [CrossRef]
8. Rączkowski, W. Aerial Archaeology. In *Encyclopedia of Global Archaeology*; Smith, C., Ed.; Springer: New York, NY, USA, 2014; pp. 33–38. ISBN 978-1-4419-0426-3.
9. Rączkowski, W. Aerial Archaeology. In *Field Archaeology from around the World*; Carver, M., Gaydarska, B., Montón-Subías, S., Eds.; SpringerBriefs in Archaeology; Springer International Publishing: Cham, Switzerland, 2015; pp. 19–25. ISBN 978-3-319-09818-0.
10. Agapiou, A.; Hadjimitsis, D.G.; Sarris, A.; Georgopoulos, A.; Alexakis, D.D. Optimum temporal and spectral window for monitoring crop marks over archaeological remains in the Mediterranean region. *J. Archaeol. Sci.* **2013**, *40*, 1479–1492. [CrossRef]
11. Neubauer, W. Images of the invisible-prospection methods for the documentation of threatened archaeological sites. *Naturwissenschaften* **2001**, *88*, 13–24. [CrossRef]
12. Beck, A.R. *Archaeological Site Detection: The Importance of Contrast*; Curran Associates, Inc.: Newcastle Upon Tyne, UK, 2008; pp. 307–312.
13. Perisset, M.C.; Tabbagh, A. Interpretation of thermal contrast on bare soils. *Archaeometry* **1981**, *23*, 169–187. [CrossRef]
14. Devereux, B.J.; Amable, G.S.; Crow, P. Visualisation of LiDAR terrain models for archaeological feature detection. *Antiquity* **2008**, *82*, 470–479. [CrossRef]
15. Challis, K.; Kokalj, Z.; Kincey, M.; Moscrop, D.; Howard, A.J. Airborne lidar and historic environment records. *Antiquity* **2008**, *82*, 1055–1064. [CrossRef]
16. Devereux, B.J.; Amable, G.S.; Crow, P.; Cliff, A.D. The potential of airborne lidar for detection of archaeological features under woodland canopies. *Antiquity* **2005**, *79*, 648–660. [CrossRef]
17. Chase, A.S.Z.; Chase, D.Z.; Chase, A.F. LiDAR for Archaeological Research and the Study of Historical Landscapes. In *Sensing the Past*; Masini, N., Soldovieri, F., Eds.; Geotechnologies and the Environment; Springer International Publishing: Cham, Switzerland, 2017; Volume 16, pp. 89–100. ISBN 978-3-319-50516-9.
18. Bennett, R.; Welham, K.; Hill, R.A.; Ford, A. A Comparison of Visualization Techniques for Models Created from Airborne Laser Scanned Data: A Comparison of Visualization Techniques for ALS Data. *Archaeol. Prospect.* **2012**, *19*, 41–48. [CrossRef]
19. Štular, B.; Kokalj, Ž.; Oštir, K.; Nuninger, L. Visualization of lidar-derived relief models for detection of archaeological features. *J. Archaeol. Sci.* **2012**, *39*, 3354–3360. [CrossRef]
20. Parcak, S.H. *Satellite Remote Sensing for Archaeology*; Routledge: London, UK; New York, NY, USA, 2009; pp. 52–103. ISBN 978-0-415-44877-2.
21. Leisz, S.J. An Overview of the Application of Remote Sensing to Archaeology during the Twentieth Century. In *Mapping Archaeological Landscapes from Space*; SpringerBriefs in Archaeology; Springer: New York, NY, USA, 2013; Volume 5, pp. 11–19. ISBN 978-1-4614-6073-2.

22. Comer, D.C. Aerial and Satellite Remote Sensing in Archaeology. In *Encyclopedia of Global Archaeology*; Smith, C., Ed.; Springer: New York, NY, USA, 2014; pp. 29–32. ISBN 978-1-4419-0426-3.
23. Kalayci, T.; Lasaponara, R.; Wainwright, J.; Masini, N. Multispectral Contrast of Archaeological Features: A Quantitative Evaluation. *Remote Sens.* **2019**, *11*, 913. [CrossRef]
24. Lambers, K. Airborne and Spaceborne Remote Sensing and Digital Image Analysis in Archaeology. In *Digital Geoarchaeology*; Siart, C., Forbriger, M., Bubenzer, O., Eds.; Natural Science in Archaeology; Springer International Publishing: Cham, Switzerland, 2018; pp. 109–122. ISBN 978-3-319-25314-5.
25. Winterbottom, S.J.; Dawson, T. Airborne multi-spectral prospection for buried archaeology in mobile sand dominated systems. *Archaeol. Prospect.* **2005**, *12*, 205–219. [CrossRef]
26. Rowlands, A.; Sarris, A. Detection of exposed and subsurface archaeological remains using multi-sensor remote sensing. *J. Archaeol. Sci.* **2007**, *34*, 795–803. [CrossRef]
27. Aqdus, S.A.; Hanson, W.S.; Drummond, J. Finding Archaeological Cropmarks: A Hyperspectral Approach. In *Remote Sensing for Environmental Monitoring, GIS Applications, and Geology VII (Vol. 6749)*; Ehlers, M., Michel, U., Eds.; SPIE: Florence, Italy, 2007.
28. Scollar, I. Archaeological Prospecting and Remote Sensing. In *Topics in Remote Sensing*; Cambridge University Press: Cambridge, UK, 1990; pp. 591–633. ISBN 978-0-521-32050-4.
29. Cool, A.C. Thermography. In *The Encyclopedia of Archaeological Sciences*; Varela, S.L., Ed.; John Wiley & Sons, Inc.: Hoboken, NJ, USA, 2018; pp. 1–5. ISBN 978-0-470-67461-1.
30. Palombo, A.; Pascucci, S.; Pergola, N.; Pignatti, S.; Santini, F.; Soldovieri, F. *Multispectral Thermal Airborne TASI-600 Data to Study the Pompeii (IT) Archaeological Area*; Copernicus Publications: Vienna, Austria, 2016; pp. 17–22.
31. Pignatti, S.; Palombo, A.; Pascucci, S.; Santini, F.; Laneve, G. *Survey of the Pompeii (IT) Archaeological Regions with the Multi-Spectral Thermal Airborne TASI Data*; Copernicus Publications: Vienna, Austria, 2017; pp. 23–28.
32. Savage, S.H.; Levy, T.E.; Jones, I.W. Prospects and problems in the use of hyperspectral imagery for archaeological remote sensing: A case study from the Faynan copper mining district, Jordan. *J. Archaeol. Sci.* **2012**, *39*, 407–420. [CrossRef]
33. Opitz, R.; Herrmann, J. Recent Trends and Long-standing Problems in Archaeological Remote Sensing. *J. Comput. Appl. Archaeol.* **2018**, *1*, 19–41. [CrossRef]
34. Schlitz, M. A review of low-level aerial archaeology and its application in Australia. *Aust. Archaeol.* **2004**, *59*, 51–58. [CrossRef]
35. Verhoeven, G.J.J. Providing an archaeological bird's-eye view—An overall picture of ground-based means to execute low-altitude aerial photography (LAAP) in Archaeology. *Archaeol. Prospect.* **2009**, *16*, 233–249. [CrossRef]
36. Martínez-del-Pozo, J.-Á.; Cerrillo-Cuenca, E.; Salas-Tovar, E. Low Altitude Aerial Photography Applications for Digital Surface Models Creation in Archaeology: Low Altitude Aerial Photography Applications. *Trans. GIS* **2013**, *17*, 227–246. [CrossRef]
37. Vilbig, J.M.; Sagan, V.; Bodine, C. Archaeological surveying with airborne LiDAR and UAV photogrammetry: A comparative analysis at Cahokia Mounds. *J. Archaeol. Sci. Rep.* **2020**, *33*, 102509. [CrossRef]
38. Barba, S.; Barbarella, M.; Di Benedetto, A.; Fiani, M.; Limongiello, M. Quality assessment of UAV photogrammetric archaeological. *Int. Arch. Photogramm. Remote Sens. Spat. Inf. Sci.* **2019**, *XLII-2/W9*, 93–100. [CrossRef]
39. Hill, A.C. Economical drone mapping for archaeology: Comparisons of efficiency and accuracy. *J. Archaeol. Sci. Rep.* **2019**, *24*, 80–91. [CrossRef]
40. Pajares, G. Overview and Current Status of Remote Sensing Applications Based on Unmanned Aerial Vehicles (UAVs). *Photogramm. Eng. Remote Sens.* **2015**, *81*, 281–330. [CrossRef]
41. Campana, S. Drones in Archaeology. State-of-the-art and Future Perspectives: Drones in Archaeology. *Archaeol. Prospect.* **2017**, *24*, 275–296. [CrossRef]
42. Searcy, M.T. Drones. In *The Encyclopedia of Archaeological Sciences*; Varela, S.L., Ed.; John Wiley & Sons, Inc.: Hoboken, NJ, USA, 2018; pp. 1–3. ISBN 978-0-470-67461-1.
43. Themistocleous, K. Themistocleous, K. The Use of UAVs for Cultural Heritage and Archaeology. In *Remote Sensing for Archaeology and Cultural Landscapes*; Hadjimitsis, D.G., Themistocleous, K., Cuca, B., Agapiou, A., Lysandrou, V., Lasaponara, R., Masini, N., Schreier, G., Eds.; Springer Remote Sensing/Photogrammetry; Springer International Publishing: Cham, Switzerland, 2020; pp. 241–269. ISBN 978-3-030-10978-3.

44. Gojda, M. Current Development in Archaeological Remote Sensing: A Central European Experience and Evaluation. *Interdiscip. Archaeol.-Nat. Sci. Archaeol.* **2019**, *X*, 155–164. [CrossRef]
45. Luo, L.; Wang, X.; Guo, H.; Lasaponara, R.; Zong, X.; Masini, N.; Wang, G.; Shi, P.; Khatteli, H.; Chen, F.; et al. Airborne and spaceborne remote sensing for archaeological and cultural heritage applications: A review of the century (1907–2017). *Remote Sens. Environ.* **2019**, *232*, 111280. [CrossRef]
46. Waagen, J. New technology and archaeological practice. Improving the primary archaeological recording process in excavation by means of UAS photogrammetry. *J. Archaeol. Sci.* **2019**, *101*, 11–20. [CrossRef]
47. López, J.; Mulero-Pázmány, M. Drones for Conservation in Protected Areas: Present and Future. *Drones* **2019**, *3*, 10. [CrossRef]
48. Singh, K.K.; Frazier, A.E. A meta-analysis and review of unmanned aircraft system (UAS) imagery for terrestrial applications. *Int. J. Remote Sens.* **2018**, *39*, 5078–5098. [CrossRef]
49. Adamopoulos, E.; Rinaudo, F. Enhancing Image-Based Multiscale Heritage Recording with Near-Infrared Data. *ISPRS Int. J. Geo-Inf.* **2020**, *9*, 269. [CrossRef]
50. Agudo, P.; Pajas, J.; Pérez-Cabello, F.; Redón, J.; Lebrón, B. The Potential of Drones and Sensors to Enhance Detection of Archaeological Cropmarks: A Comparative Study between Multi-Spectral and Thermal Imagery. *Drones* **2018**, *2*, 29. [CrossRef]
51. Barazzetti, L.; Brumana, R.; Oreni, D.; Cuca, B.; Previtali, M.; Roncoroni, F. Finding Buried Remains Using Thermal Images. *Int. J. Herit. Digit. Era* **2015**, *4*, 295–306. [CrossRef]
52. Brooke, C.; Clutterbuck, B. Mapping Heterogeneous Buried Archaeological Features Using Multisensor Data from Unmanned Aerial Vehicles. *Remote Sens.* **2019**, *12*, 41. [CrossRef]
53. Brumana, R.; Oreni, D.; Van Hecke, L.; Barazzetti, L.; Previtali, M.; Roncoroni, F.; Valente, R. Combined geometric and thermal analysis from UAV platforms for archaeological heritage documenation. *ISPRS Ann. Photogramm. Remote Sens. Spat. Inf. Sci.* **2013**, *II-5/W1*, 49–54. [CrossRef]
54. Calleja, J.F.; Pagés, O.R.; Díaz-Álvarez, N.; Peón, J.; Gutiérrez, N.; Martín-Hernández, E.; Relea, A.C.; Melendi, D.R.; Álvarez, P.F. Detection of buried archaeological remains with the combined use of satellite multispectral data and UAV data. *Int. J. Appl. Earth Obs. Geoinf.* **2018**, *73*, 555–573. [CrossRef]
55. Casana, J.; Kantner, J.; Wiewel, A.; Cothren, J. Archaeological aerial thermography: A case study at the Chaco-era Blue J community, New Mexico. *J. Archaeol. Sci.* **2014**, *45*, 207–219. [CrossRef]
56. Casana, J.; Wiewel, A.; Cool, A.; Hill, A.C.; Fisher, K.D.; Laugier, E.J. Archaeological Aerial Thermography in Theory and Practice. *Adv. Archaeol. Pr.* **2017**, *5*, 310–327. [CrossRef]
57. Casella, V.; Franzini, M.; Gorrini, M.E. Crop marks detection through optical and multi-spectral imagery acquired by UAV. In Proceedings of the 2018 Metrology for Archaeology and Cultural Heritage (MetroArchaeo), Cassino, Italy, 22–24 October 2018; pp. 173–177.
58. Chelmus, A.; Radvan, R.; Angheluta, L. Aerial Investigations Corroboration for Archaeology and Monuments. In Proceedings of the 2018 11th International Conference on Developments in eSystems Engineering (DeSE), Cambridge, UK, 2–5 September 2018; pp. 113–116.
59. Colombatti, G.; Aboudan, A.; Bettanini, C.; Magnini, L.; Bettineschi, C.; Deotto, G.; Toninello, L.; Debei, S.; Guio, A.D.; Zanovello, P.; et al. Horus—A drone project for visual and IR imaging. In Proceedings of the 2017 IEEE International Workshop on Metrology for AeroSpace (MetroAeroSpace), Padua, Italy, 21–23 June 2017; pp. 589–592.
60. Cowley, D.; Moriarty, C.; Geddes, G.; Brown, G.; Wade, T.; Nichol, C. UAVs in Context: Archaeological Airborne Recording in a National Body of Survey and Record. *Drones* **2017**, *2*, 2. [CrossRef]
61. De Reu, J.; Trachet, J.; Laloo, P.; De Clercq, W. From Low Cost UAV Survey to High Resolution Topographic Data: Developing our Understanding of a Medieval Outport of Bruges: From Low Cost UAV Survey to High Resolution Topographic Data. *Archaeol. Prospect.* **2016**, *23*, 335–346. [CrossRef]
62. Evers, R.; Masters, P. The application of low-altitude near-infrared aerial photography for detecting clandestine burials using a UAV and low-cost unmodified digital camera. *Forensic Sci. Int.* **2018**, *289*, 408–418. [CrossRef] [PubMed]
63. Faltýnová, M.; Pavelka, K.; Nový, P.; Šedina, J. Complex Archaeological Prospection Using Combination of Non-destructive Techniques. *Int. Arch. Photogramm. Remote Sens. Spat. Inf. Sci.* **2015**, *XL-5/W7*, 141–146. [CrossRef]

64. Fenger-Nielsen, R.; Hollesen, J.; Matthiesen, H.; Andersen, E.A.S.; Westergaard-Nielsen, A.; Harmsen, H.; Michelsen, A.; Elberling, B. Footprints from the past: The influence of past human activities on vegetation and soil across five archaeological sites in Greenland. *Sci. Total Environ.* **2019**, *654*, 895–905. [CrossRef]
65. Fernández-Lozano, J.; Gutiérrez-Alonso, G. Improving archaeological prospection using localized UAVs assisted photogrammetry: An example from the Roman Gold District of the Eria River Valley (NW Spain). *J. Archaeol. Sci. Rep.* **2016**, *5*, 509–520. [CrossRef]
66. González, J.F.; Hernández, F.V. NDVI Identification and Survey of a Roman Road in the Northern Spanish Province of Álava. *Remote Sens.* **2019**, *11*, 725. [CrossRef]
67. Garzia, F.; Lombardi, M.; Papi, L. Analysis and data acquisition methodology based on flying drones for the implementation of the internet of everything to smart archaeological areas. *Int. J. Herit. Arch. Stud. Repairs Maintence* **2017**, *2*, 383–394. [CrossRef]
68. Gehrke, R.; Greiwe, A. RGBI images with UAV and off-the-shelf compact cameras: An investigation of linear sensor characteristics. *EARSel eProc.* **2014**, *13*, 53–58.
69. Gini, R.; Passoni, D.; Pinto, L.; Sona, G.; Pulejo, S.; Baracani, M. UAV-Based Images for a Documentation and Active Fruition of the Natural and Cultural Heritage. *Boll. AIC* **2012**, *144*, 167–181.
70. González, J.J.F.; González, J.I.F. Prospección arqueológica en NDVI con drones. El uso de geoEuskadi como herramienta de ponderación de un nuevo método. *Rev. Mapp.* **2018**, *29*, 24–29.
71. Hill, A.C.; Laugier, E.J.; Casana, J. Archaeological Remote Sensing Using Multi-Temporal, Drone-Acquired Thermal and Near Infrared (NIR) Imagery: A Case Study at the Enfield Shaker Village, New Hampshire. *Remote Sens.* **2020**, *12*, 690. [CrossRef]
72. Hill, A.C.; Rowan, Y.; Kersel, M.M. Mapping with Aerial Photographs: Recording the Past, the Present, and the Invisible at Marj Rabba, Israel. *Near East. Archaeol.* **2014**, *77*, 182–186. [CrossRef]
73. Khan, S.; Aragão, L.; Iriarte, J. A UAV–lidar system to map Amazonian rainforest and its ancient landscape transformations. *Int. J. Remote Sens.* **2017**, *38*, 2313–2330. [CrossRef]
74. Korczyńska, M.; Cappenberg, K.; Nowak, M.; Szwarczewski, P.; Hoyo, M.M. Multi-methodological approaches to investigate large archaeological sites: The case study of the Eneolithic settlement in Mozgawa, western Lesser Poland. *J. Archaeol. Sci. Rep.* **2019**, *27*, 101941. [CrossRef]
75. Koucká, L.; Kopačková, V.; Fárová, K.; Gojda, M. UAV Mapping of an Archaeological Site Using RGB and NIR High-Resolution Data. *Proceedings* **2018**, *2*, 351. [CrossRef]
76. Lehmann, J.R.K.; Smithson, K.Z.; Prinz, T. Making the invisible visible: Using UAS-based high-resolution color-infrared imagery to identify buried medieval monastery walls. *J. Unmanned Veh. Syst.* **2015**, *3*, 58–67. [CrossRef]
77. Levin, S.; Yuan, M.; Adler, M. Thermographic Quantification for Archaeological Prospection at Picuris Pueblo, New Mexico. In Proceedings of the 2018 3rd Digital Heritage International Congress (DigitalHERITAGE) held jointly with 2018 24th International Conference on Virtual Systems & Multimedia (VSMM 2018), San Francisco, CA, USA, 26–30 October 2018; pp. 1–8.
78. Liu, C.; Cao, Y.; Yang, C.; Zhou, Y.; Ai, M. Pattern identification and analysis for the traditional village using low altitude UAV-borne remote sensing: Multifeatured geospatial data to support rural landscape investigation, documentation and management. *J. Cult. Herit.* **2020**, *44*, 185–195. [CrossRef]
79. Magnini, L.; Bettineschi, C.; De Guio, A.; Burigana, L.; Colombatti, G.; Bettanini, C.; Aboudan, A. Multisensor-multiscale approach in studying the proto-historic settlement of Bostel in northern Italy. *Archeol. Calc.* **2019**, *30*, 347–365. [CrossRef]
80. Malinverni, E.S.; Barbaro, C.C.; Pierdicca, R.; Bozzi, C.A.; Tassetti, A.N. UAV Surveying for a complete mapping and documentation of archaeological findings. The early neolithic site of Portonovo. *Int. Arch. Photogramm. Remote Sens. Spat. Inf. Sci.* **2016**, *XLI-B1*, 1149–1155. [CrossRef]
81. Masini, N.; Marzo, C.; Manzari, P.; Belmonte, A.; Sabia, C.; Lasaponara, R. On the characterization of temporal and spatial patterns of archaeological crop-marks. *J. Cult. Herit.* **2018**, *32*, 124–132. [CrossRef]
82. Mather, A.; Fyfe, R.; Clason, C.; Stokes, M.; Mills, S.; Barrows, T. Automated mapping of relict patterned ground: An approach to evaluate morphologically subdued landforms using unmanned-aerial-vehicle and structure-from-motion technologies. *Prog. Phys. Geogr. Earth Environ.* **2019**, *43*, 174–192. [CrossRef]
83. Matoušková, E.; Starková, L.; Pavelka, K.; Nováček, K.; Šedina, J.; Faltýnová, M.; Housarová, E. Using remote sensing data for documentation of archaeological sites in northwestern Mesopotamia. *Int. Arch. Photogramm. Remote Sens. Spat. Inf. Sci.* **2016**, *XLI-B5*, 335–342. [CrossRef]

84. McLeester, M.; Casana, J.; Schurr, M.R.; Hill, A.C.; Wheeler, J.H. Detecting prehistoric landscape features using thermal, multi-spectral, and historical imagery analysis at Midewin National Tallgrass Prairie, Illinois. *J. Archaeol. Sci. Rep.* **2018**, *21*, 450–459. [CrossRef]
85. Ramón, A.G.M.; Barba, L.; Ortiz, A.; Blancas, J. Geophysical prospection at the formative site of Altica in the Teotihacan Valley Piedmont. *Anc. Mesoam.* **2019**, *30*, 267–278. [CrossRef]
86. Moriarty, C.; Cowley, D.C.; Wade, T.; Nichol, C.J. Deploying multi-spectral remote sensing for multi-temporal analysis of archaeological crop stress at Ravenshall, Fife, Scotland. *Archaeol. Prospect.* **2019**, *26*, 33–46. [CrossRef]
87. Murtha, T.M.; Broadbent, E.N.; Golden, C.; Scherer, A.; Schroder, W.; Wilkinson, B.; Zambrano, A.A. Drone-Mounted Lidar Survey of Maya Settlement and Landscape. *Lat. Am. Antiq.* **2019**, *30*, 630–636. [CrossRef]
88. O'Driscoll, J. Landscape applications of photogrammetry using unmanned aerial vehicles. *J. Archaeol. Sci. Rep.* **2018**, *22*, 32–44. [CrossRef]
89. Parisi, E.I.; Suma, M.; Güleç Korumaz, A.; Rosina, E.; Tucci, G. Aerial platforms (UAV) surveys in the VIS and TIR range. Applications on archaeology and agriculture. *Int. Arch. Photogramm. Remote Sens. Spat. Inf. Sci.* **2019**, *XLII-2/W11*, 945–952. [CrossRef]
90. Pavelka, K.; Šedina, J.; Matoušková, E. High Resolution Drone Surveying of the Pista Geoglyph in Palpa, Peru. *Geosciences* **2018**, *8*, 479. [CrossRef]
91. González, M.E.P.; Revilla, J.I.G. A new environmental and spatial approach to the Tiwanaku World Heritage site (Bolivia) using remote sensing (UAV and satellite images). *Geoarchaeology* **2020**, *35*, 416–429. [CrossRef]
92. Pisz, M.; Tomas, A.; Hegyi, A. Non-destructive research in the surroundings of the Roman Fort Tibiscum (today Romania). *Archaeol. Prospect.* **2020**. [CrossRef]
93. Poirier, N. From Archaeological Evidence for Agricultural Manuring to an Understanding of Settlement and Landscape Dynamics—An Experiment in Non-Invasive Archaeological Methods Undertaken in South-West France. In *Materialien zur Bodendenkmalpflege im Rheinland 26*; Keller, C., Wohlfarth, C., Eds.; LVR-Amt für Bodendenkmalpflege im Rheinland: Cologne, Germany, 2018; pp. 41–58.
94. Poirier, N.; Hautefeuille, F.; Calastrenc, C. Low Altitude Thermal Survey by Means of an Automated Unmanned Aerial Vehicle for the Detection of Archaeological Buried Structures: Thermal Archaeological Survey by Automated Unmanned Aerial Vehicle. *Archaeol. Prospect.* **2013**, *20*, 303–307. [CrossRef]
95. Poirier, N.; Hautefeuille, F.; Calastrenc, C. L'utilisation des micro-drones pour la prospection archéologique à basse altitude. *Rev. Fr. Photogramm. Télédétect.* **2017**, *213*, 81–94.
96. Poscetti, V.; Malatesta, S.G.; Cirilli, V.; Lella, F.; Rondinelli, V.; Esposito, S.; Balsi, M. Preliminary results of the Castelmonardo Project. *Archeol. Calc.* **2017**, *28*, 391–402. [CrossRef]
97. Raeva, P.; Pavelka, K.; Hanuš, J.; Gojda, M. Using of both hyperspectral aerial sensing and RPAS multi-spectral sensing for potential archaeological sites detection. In *Multispectral, Hyperspectral, and Ultraspectral Remote Sensing Technology, Techniques and Applications VII*; Larar, A.M., Suzuki, M., Wang, J., Eds.; SPIE: Honolulu, HI, USA, 2018; p. 47.
98. Risbøl, O.; Gustavsen, L. LiDAR from drones employed for mapping archaeology—Potential, benefits and challenges. *Archaeol. Prospect.* **2018**, *25*, 329–338. [CrossRef]
99. Carmona, J.Á.S.; Quirós, E.; Mayoral, V.; Charro, C. Assessing the potential of multi-spectral and thermal UAV imagery from archaeological sites. A case study from the Iron Age hillfort of Villasviejas del Tamuja (Cáceres, Spain). *J. Archaeol. Sci. Rep.* **2020**, *31*, 102312. [CrossRef]
100. Saunaluoma, S.; Anttiroiko, N.; Moat, J. UAV survey at archaeological earthwork sites in the Brazilian state of Acre, southwestern Amazonia. *Archaeol. Prospect.* **2019**, *26*, 325–331. [CrossRef]
101. Šedina, J.; Pavelka, K.; Housarová, E. Archaeological documentation of a defunct Iraqi town. *Int. Arch. Photogramm. Remote Sens. Spat. Inf. Sci.* **2016**, *XLI-B1*, 1031–1035. [CrossRef]
102. Šedina, J.; Housarová, E.; Matoušková, E. Documentation of Urn Graves of Knovíz Culture by RPAS. *Geoinformatics Fce Ctu* **2016**, *15*, 71–82. [CrossRef]
103. Šedina, J.; Housarová, E.; Raeva, P. Using RPAS for the detection of archaeological objects using multi-spectral and thermal imaging. *Eur. J. Remote. Sens.* **2019**, *52*, 182–191. [CrossRef]
104. Šedina, J.; Hůlková, M.; Pavelka, K.; Pavelka, K., Jr. RPAS for documentation of Nazca aqueducts. *Eur. J. Remote. Sens.* **2019**, *52*, 174–181. [CrossRef]

105. Šedina, J.; Pavelka, K.; Housarová, E. RPAS as a tool for mapping and other special work. In *Advances and Trends in Engineering Sciences and Technologies, Proceedings of the International Conference on Engineering Sciences and Technologies, Tatranská Štrba, Slovak Republic, 27–29 May 2015*; Ali, M., Platko, P., Eds.; CRC Press: Boca Raton, FL, USA, 2015; pp. 405–412. ISBN 978-1-138-02907-1.
106. Skarlatos, D.; Vlachos, M. Vegetation removal from UAV derived DSMs, using combination of RGB and NIR imagery. *ISPRS Ann. Photogramm. Remote Sens. Spat. Inf. Sci.* **2018**, *IV-2*, 255–262. [CrossRef]
107. Thomas, H. Some like it hot: The impact of next generation FLIR Systems thermal cameras on archaeological thermography. *Archaeol. Prospect.* **2018**, *25*, 81–87. [CrossRef]
108. Thomas, H.; Williams, E. High resolution terrestrial thermography of archaeological sites. *Archaeol. Prospect.* **2019**, *26*, 189–198. [CrossRef]
109. Uribe, P.; Angás, J.; Pérez-Cabello, F. Aerial mapping and multi-sensor approaches from remote sensing applied to the Roman Archaeological Heritage. *Int. Arch. Photogramm. Remote Sens. Spat. Inf. Sci.* **2015**, *XL-5/W4*, 461–467. [CrossRef]
110. VanValkenburgh, P.; Cushman, K.C.; Butters, L.J.C.; Vega, C.R.; Roberts, C.B.; Kepler, C.; Kellner, J. Lasers Without Lost Cities: Using Drone Lidar to Capture Architectural Complexity at Kuelap, Amazonas, Peru. *J. Field Archaeol.* **2020**, *45*, S75–S88. [CrossRef]
111. Walker, S. Low-altitude aerial thermography for the archaeological investigation of arctic landscapes. *J. Archaeol. Sci.* **2020**, *117*, 105126. [CrossRef]
112. Zhou, W.; Chen, F.; Guo, H.; Hu, M.; Li, Q.; Tang, P.; Zheng, W.; Liu, J.; Luo, R.; Yan, K.; et al. UAV Laser scanning technology: A potential cost-effective tool for micro-topography detection over wooded areas for archaeological prospection. *Int. J. Digit. Earth* **2020**, *1*, 1–23. [CrossRef]
113. Sonnemann, T.; Hung, J.U.; Hofman, C. Mapping Indigenous Settlement Topography in the Caribbean Using Drones. *Remote Sens.* **2016**, *8*, 791. [CrossRef]
114. Megarry, W.; Graham, C.; Gilhooly, B.; O'Neill, B.; Sands, R.; Nyland, A.; Cooney, G. Debitage and Drones: Classifying and Characterising Neolithic Stone Tool Production in the Shetland Islands Using High Resolution Unmanned Aerial Vehicle Imagery. *Drones* **2018**, *2*, 12. [CrossRef]
115. Jorayev, G.; Wehr, K.; Benito-Calvo, A.; Njau, J.; de la Torre, I. Imaging and photogrammetry models of Olduvai Gorge (Tanzania) by Unmanned Aerial Vehicles: A high-resolution digital database for research and conservation of Early Stone Age sites. *J. Archaeol. Sci.* **2016**, *75*, 40–56. [CrossRef]
116. Parcero-Oubiña, C.; Fábrega-Álvarez, P.; Salazar, D.; Troncoso, A.; Hayashida, F.; Pino, M.; Borie, C.; Echenique, E. Ground to air and back again: Archaeological prospection to characterize prehispanic agricultural practices in the high-altitude Atacama (Chile). *Quat. Int.* **2017**, *435*, 98–113. [CrossRef]
117. Colomina, I.; Molina, P. Unmanned aerial systems for photogrammetry and remote sensing: A review. *Isprs J. Photogramm. Remote Sens.* **2014**, *92*, 79–97. [CrossRef]
118. Qi, S.; Wang, F.; Jing, L. Unmanned Aircraft System Pilot/Operator Qualification Requirements and Training Study. *Matec Web Conf.* **2018**, *179*, 03006. [CrossRef]
119. Jeziorska, J. UAS for Wetland Mapping and Hydrological Modeling. *Remote Sens.* **2019**, *11*, 1997. [CrossRef]
120. Forlani, G.; Dall'Asta, E.; Diotri, F.; di Cella, U.M.; Roncella, R.; Santise, M. Quality Assessment of DSMs Produced from UAV Flights Georeferenced with On-Board RTK Positioning. *Remote Sens.* **2018**, *10*, 311. [CrossRef]
121. Tomaštík, J.; Mokroš, M.; Surový, P.; Grznárová, A.; Merganič, J. UAV RTK/PPK Method—An Optimal Solution for Mapping Inaccessible Forested Areas? *Remote Sens.* **2019**, *11*, 721. [CrossRef]
122. Verhoeven, G.J. Near-Infrared Aerial Crop Mark Archaeology: From its Historical Use to Current Digital Implementations. *J. Archaeol. Method. Theory* **2012**, *19*, 132–160. [CrossRef]
123. Aroma, R.J.; Raimond, K.; Razmjooy, N.; Estrela, V.V.; Hemanth, J. Multispectral vs hyperspectral imaging for unmanned aerial vehicles: Current and prospective state of affairs. In *Imaging and Sensing for Unmanned Aircraft Systems: Volume 2: Deployment and Applications*; Estrela, V.V., Hemanth, J., Saotome, O., Nikolakopoulos, G., Sabatini, R., Eds.; Institution of Engineering and Technology: London, UK, 2020; pp. 133–155. ISBN 978-1-78561-644-0.
124. Linford, N. The application of geophysical methods to archaeological prospection. *Rep. Prog. Phys.* **2006**, *69*, 2205–2257. [CrossRef]
125. Gaffney, C. Detecting trends in the prediction of the buried past: A review of geophysical techniques in archaeology. *Archaeometry* **2008**, *50*, 313–336. [CrossRef]

126. Garcia-Fernandez, M.; Alvarez-Lopez, Y.; Heras, F.L.; Gonzalez-Valdes, B.; Rodriguez-Vaqueiro, Y.; Pino, A.; Arboleya-Arboleya, A. GPR system on-board a UAV for non-invasive detection of buried objects. In Proceedings of the 2018 IEEE International Symposium on Antennas and Propagation & USNC/URSI National Radio Science Meeting, Boston, MA, USA, 8–13 July 2018; pp. 1967–1968.
127. Ludeno, G.; Catapano, I.; Renga, A.; Vetrella, A.R.; Fasano, G.; Soldovieri, F. Assessment of a micro-UAV system for microwave tomography radar imaging. *Remote Sens. Environ.* **2018**, *212*, 90–102. [CrossRef]
128. Schartel, M.; Burr, R.; Mayer, W.; Docci, N.; Waldschmidt, C. UAV-Based Ground Penetrating Synthetic Aperture Radar. In Proceedings of the 2018 IEEE MTT-S International Conference on Microwaves for Intelligent Mobility (ICMIM), Munich, Germany, 16–18 April 2018; pp. 1–4.
129. Guyot, A.; Hubert-Moy, L.; Lorho, T. Detecting Neolithic Burial Mounds from LiDAR-Derived Elevation Data Using a Multi-Scale Approach and Machine Learning Techniques. *Remote Sens.* **2018**, *10*, 225. [CrossRef]
130. Soroush, M.; Mehrtash, A.; Khazraee, E.; Ur, J.A. Deep Learning in Archaeological Remote Sensing: Automated Qanat Detection in the Kurdistan Region of Iraq. *Remote Sens.* **2020**, *12*, 500. [CrossRef]
131. Orengo, H.A.; Conesa, F.C.; Garcia-Molsosa, A.; Lobo, A.; Green, A.S.; Madella, M.; Petrie, C.A. Automated detection of archaeological mounds using machine-learning classification of multisensor and multitemporal satellite data. *Proc. Natl. Acad. Sci. USA* **2020**, *117*, 18240–18250. [CrossRef] [PubMed]
132. Gould, R.A. Archaeological Survey by Air: A Case from the Australian Desert. *J. Field Archaeol.* **1987**, *14*, 431–443.
133. Zakharov, A.O. A View from the Highlands: Archaeology and Settlement History of West Sumatra, Indonesia, by Mai Lin Tjoa-Bonatz. *J. Malays. Branch R. Asiat. Soc.* **2020**, *93*, 169–171. [CrossRef]
134. Oczipka, M.; Bemmann, J.; Piezonka, H.; Munkabayar, J.; Ahrens, B.; Achtelik, M.; Lehmann, F. Small Drones for Geo-Archaeology in the Steppe: Locating and Documenting the Archaeological Heritage of the Orkhon Valley in Mongolia. In *Remote Sensing for Environmental Monitoring, GIS Applications, and Geology VII (Vol. 6749)*; Michel, U., Civco, D.L., Eds.; SPIE: Berlin, Germany, 2009; p. 747806.
135. Rouse, L.M.; Krumnow, J. On the fly: Strategies for UAV-based archaeological survey in mountainous areas of Central Asia and their implications for landscape research. *J. Archaeol. Sci. Rep.* **2020**, *30*, 102275. [CrossRef]